Elsevier Editorial System(tm) for Geochimica et Cosmochimica Acta

Manuscript Draft

Manuscript Number: GCA-D-17-00504R2

Title: Screening apatites for (U-Th)/He thermochronometry via continuous ramped heating: Helium age components and implications for age dispersion

Article Type: Article

Corresponding Author: Dr. Kalin T. McDannell, Ph.D.

Corresponding Author's Institution: Lehigh University

First Author: Kalin T. McDannell, Ph.D.

Order of Authors: Kalin T. McDannell, Ph.D.; Peter K Zeitler, Ph.D.; Darwin G Janes, M.S.; Bruce D Idleman, Ph.D.; Annia K Fayon, Ph.D.

Abstract: Old slowly-cooled apatites often yield dispersed (U-Th)/He ages for a variety of reasons, some well understood and some not. Analytical protocols like careful grain selection can reduce the impact of this dispersion but add costs in time and resources and too often have proven insufficient. We assess a new analytical protocol that utilizes static-gas measurement during continuous ramped heating (CRH) as a means to rapidly screen apatite samples. In about the time required for a conventional total-gas analysis, this method can discriminate between samples showing expected volume-diffusion behavior and those showing anomalous release patterns inconsistent with their direct use in thermochronologic applications. This method also appears able to discriminate between the radiogenic and extraneous 4He fractions released by a sample, potentially allowing ages to be corrected.

Well-behaved examples such as the Durango standard and other apatites with good age reproducibility show the expected smooth, sigmoidal gas-release curves predicted for volume diffusion using typical apatite kinetics, with complete exhaustion by ~900°C for linear heating at 20°C/minute. Secondary factors such as U and Th zoning and alpha-loss distribution have a relatively minor impact on such profiles. In contrast, samples having greater age dispersion show significant He release in the form of outgassing spikes and He release deferred to higher temperatures. Screening results for a range of samples permit us to assess the degree to which CRH screening can identify misbehaving grains, give insight into the source of extraneous He, and suggest that in some cases it may be possible to correct ages for the presence of such components.

Screening apatites for (U-Th)/He thermochronometry via continuous ramped heating: He age components and implications for age dispersion

Kalin T. McDannell[a,b]*, Peter K. Zeitler[a], Darwin G. Janes[a], Bruce D. Idleman[a], and Annia K. Fayon[b,c]

[a]*Department of Earth and Environmental Sciences, Lehigh University, Bethlehem, PA 18015*
[b]*Geological Survey of Canada, Natural Resources Canada, Calgary, AB T2L 2A7*
[c]*Department of Earth Sciences, University of Minnesota, Minneapolis, MN 55455*

*Corresponding author: kmcdannell@gmail.com; kalin.mcdannell@canada.ca

Keywords: apatite, screening, dispersion, He, diffusion, thermochronology

ABSTRACT

Old slowly-cooled apatites often yield dispersed (U-Th)/He ages for a variety of reasons, some well understood and some not. Analytical protocols like careful grain selection can reduce the impact of this dispersion but add costs in time and resources and too often have proven insufficient. We assess a new analytical protocol that utilizes static-gas measurement during continuous ramped heating (CRH) as a means to rapidly screen apatite samples. In about the time required for a conventional total-gas analysis, this method can discriminate between samples showing expected volume-diffusion behavior and those showing anomalous release patterns inconsistent with their direct use in thermochronologic applications. This method also appears able to discriminate between the radiogenic and extraneous ^{4}He fractions released by a sample, potentially allowing ages to be corrected.

Well-behaved examples such as the Durango standard and other apatites with good age reproducibility show the expected smooth, sigmoidal gas-release curves predicted for volume diffusion using typical apatite kinetics, with complete exhaustion by ~900°C for linear heating at 20°C/minute. Secondary factors such as U and Th zoning and alpha-loss distribution have a relatively minor impact on such profiles. In contrast, samples having greater age dispersion show significant He release in the form of outgassing spikes and He release deferred to higher temperatures. Screening results for a range of samples permit us to assess the degree to which CRH screening can identify misbehaving grains, give insight into the source of extraneous He,

and suggest that in some cases it may be possible to correct ages for the presence of such components.

1. Introduction

Since the suggestion that (U-Th)/He ages of apatite might function as a thermochronometer (Zeitler et al., 1987), many advances have been made in documenting the fundamental diffusion systematics of He in this phase (e.g., Farley et al., 1996; Wolf et al., 1996; Warnock et al., 1997; Farley, 2000; Shuster et al., 2006). These advances include understanding that the diffusion length scale appears to be the physical grain dimension, quantifying the alpha-ejection process and means of correcting for it, measuring the range of diffusion kinetics seen in natural samples, and assessing the impact that zoning in U and Th can have on measured apatite He ages. More recently, it has been shown that radiation damage (Shuster et al., 2006; Flowers et al., 2009) can act as an important control on diffusivity, with damage acting to impede diffusion.

Despite this progress, work on sample suites from different geologic settings, (e.g. Fitzgerald et al., 2006; Peyton et al., 2012) has shown that datasets often exhibit age dispersion beyond what radiation damage, grain size, and zoning can explain. Other documented factors that can lead to age dispersion include He implantation, (Spiegel et al., 2009), U-Th-rich grain boundary phases, (Murray et al., 2014), fluid and mineral inclusions, (Farley, 2002; Vermeesch et al., 2007), and broken grains (Beucher et al., 2013; Brown et al., 2013). In some cases, quantification of these factors has led to not only more sophisticated explanations for dispersed data but also the ability to extract additional thermal-history information (Green et al., 2006; Flowers and Kelley, 2011). However, in many cases unexplained dispersion remains. Most recently, extrapolating from the impact that radiation damage has on diffusion kinetics, attention has turned to crystal imperfections ranging across spatial scales from substitutions associated with variable chemical composition (Djimbi et al., 2015), deformation-induced microstructures (Fayon and Hansen, 2015), vacancy damage (Gerin et al., 2017), or crystallographic voids (Zeitler et al., 2017). All these explanations still leave the practical challenge of conducting time- and cost-effective analyses by identifying issues as early as possible in the analytical process, certainly before ages are calculated and samples become part of a statistical pool.

Here we take an empirical approach to the problem of age dispersion and assess an alternative experimental method for characterizing ^{4}He components in apatite. The continuous ramped heating (CRH) method (Idleman and Zeitler, 2014; McDannell et al., 2015; McDannell, 2017; Idleman et al., 2017) employs continuous heating and static-mode measurement of evolved gas. This technique permits efficient screening of apatite samples through characterization of diffusive loss during heating because an entire diffusion experiment can be carried out in the same time as is required for a conventional gas extraction and second "re-extract" step. Continuously heated samples that outgas by volume diffusion (VD) during a linear heating schedule produce characteristic sigmoidal ^{4}He cumulative-loss curves, with factors such as alpha-ejection and parent isotope zoning leading to only subtle though identifiable changes in the form of the sigmoidal release curve. In contrast, we find that anomalous samples with poor single-grain age reproducibility commonly yield complex cumulative-loss curves that show abrupt steps, multiple inflection points, or displacement in temperature from those of other apatites analyzed under the same experimental conditions. We conclude that (1) reliable, well-replicated ages require simple CRH outgassing behavior, (2) CRH analysis provides a robust means of eliminating ill-behaved samples from data sets, and (3) in some cases, screening results can be used to correct ages to account for extraneous ^{4}He components.

2. Continuous Ramped Heating (CRH) Method and Sample Assessment

2.1 Analytical Procedures

Apatite samples for ^{4}He analysis via the CRH method were obtained using standard processing: crushing, sieving, and density- and magnetic-separation procedures. All grains were picked under a Nikon SMZ800 microscope at ~95x magnification and (except for the solubility samples) were then examined under an Olympus BH2-UMA polarized petrographic microscope to inspect for inclusions at up to 500x. Grains were digitally photographed in order to record their 3D sizes and shapes for determination of alpha-correction factors. Individual grains were placed in small niobium microtubes whose ends were crimped, and then loaded into the extraction system's sample dropper that permits multiple samples to be readied for sequential analysis in a resistance furnace. Samples were degassed of their ^{4}He in the Lehigh University noble-gas laboratory and parent U-Th-Sm isotopes were subsequently measured by dissolution

and isotope dilution of sample aliquots by ICP-MS at the laboratory of Dr. Peter Reiners at the University of Arizona following the procedures of Reiners and Nicolescu (2006).

The He extraction line ^{4}He blank is typically 1 x 10^{-16} moles or less for conventional analyses, however for the CRH technique the cumulative hot blank is generally between ~1 x 10^{-15} to ~1 x 10^{-14} moles because of the extended duration of the experiment. The relative contribution of blank varies during heating but generally is trivial, at most a few percent of the total gas in the earliest heating steps (Idleman et al., 2017). ^{4}He amounts are measured by manometric peak-height comparison against ^{4}He from pipetted aliquots of the mass-discrimination standard. For conventional analyses this approach agrees to better than 1% with sample amounts determined using our ^{3}He spike, and is preferred because under high hydrogen loads (beams >10^{-9} A) we have found ^{3}He spike determinations become unreliable due to interferences at m/e=3. Typical variations in ^{4}He sensitivity (mol/A) over the course of a day are about 0.5%.

Apatite samples were outgassed using a water-cooled double-vacuum resistance furnace that was held idle at 200°C between runs. Each sample was heated using a highly repeatable, linearly ramped, rate-controlled heating schedule from 200°C to 1150°C at a rate of 20°C/minute. However, while we found the ramped heating to be precise, experiments using an internal thermocouple showed the presence of both an absolute temperature offset of up to ~55°C during early heating, as well as a time lag related to the thermal inertia of the crucible. All quoted temperatures in data tables are corrected for these effects (raw temperatures are shown in the supplement), and because the time lag varies with heating rate, we were careful that all runs were conducted under the same conditions (i.e. beginning heating from a crucible stabilized at 200˚C and ramping at exactly 20°C/minute).

During CRH experiments, sample data (cumulative time and ^{4}He signal) were collected using a Pfeiffer Prisma QMS 200 quadrupole mass spectrometer every 21.5 s over ~130 data blocks. SAES GP50 getters in the extraction line and in the mass spectrometer volume sorb active gases during heating while the degassed He from apatite grains was measured. Due to significant hydrogen release at furnace temperatures between 400-600°C, in a few cases depression of the true measured ^{4}He signal at high temperature occurred, along with apparent sensitivity hysteresis

(Lieszkovszky et al., 1990). To alleviate these effects, between runs the furnace was allowed to cool back to 200°C over one hour, also permitting the quadrupole sensitivity to settle. In addition, every two to four sample runs the furnace went through extended outgassing at 1350°C. To better and more directly address possible sensitivity variations, for samples run subsequent to the Mongolian suite, we began injecting a calibrated shot of ^{4}He shot as soon as the ^{4}He signal stabilized at the end of runs, so that we could use the method of standard additions to determine sample amounts.

2.2 Data reduction

Individual mass spectrometer measurements were treated mathematically as the result of square-pulse heating steps using the average temperature experienced by the sample during the measurement cycle. Raw mass spectrometer data-acquisition times were equated to temperature using the heating ramp rate of 20°C/minute (~7.5°C per analytical block) in combination with the empirical temperature calibration of crucible (see above). Raw ^{4}He measurements were translated to cumulative fractional loss, *f,* and then numerically differentiated to obtain incremental fractional loss per temperature step, *df* (Fig. 1). The *f*-curve displays the cumulative liberation of ^{4}He that progresses with increasing temperature (normalized to unity), while the *df* spectrum shows the normalized rate of gas release as a function of temperature (this will be specific to the given heating rate). We refrain from reporting sample-specific kinetic parameters because of the potential inaccuracies in the furnace temperatures; going forward such work would best be done using a laser heating system (Idleman et al., 2017; McDannell, 2017).

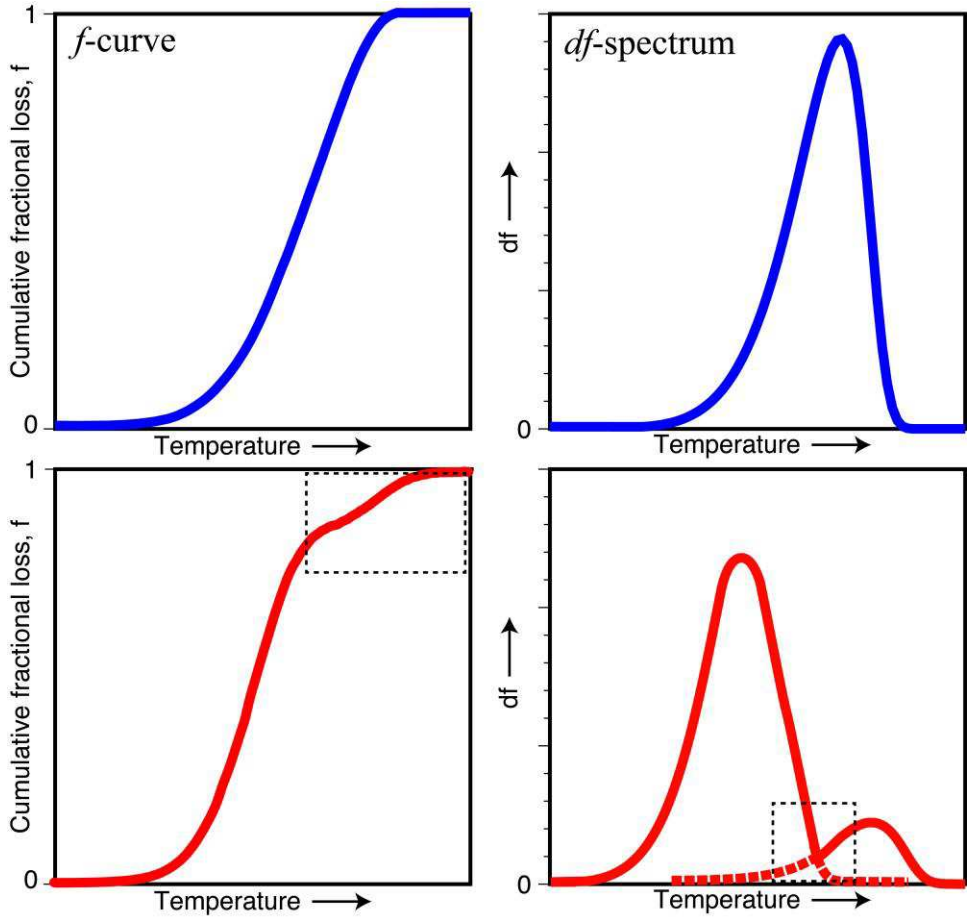

Figure 1. Schematic sigmoidal shape of a smooth cumulative fractional loss (*f*-curve; top left) for expected behavior that is then differentiated to produce a *df* spectrum (top right). Bottom shows the *f*-curve and *df* spectrum for a hypothetical sample showing anomalous behavior, in this case a flattened high-temperature *f*-curve which manifests in the *df* spectrum as a secondary release at the peak shoulder (dashed box). This example would be a candidate for age correction (see section 2.4) where the observed data are honored up to the second minor peak, which is then removed using a peak fit through the lower-temperature data.

2.3 Expected behavior

In general, He diffusion in apatite obeys thermally-activated volume diffusion (modified by radiation-damage effects) where the crystal size is the diffusion domain (Farley, 2000) and He outgassing produces a simple, smooth, sigmoidal release curve. All else kept constant, increasing the activation energy (E_a) will narrow a peak on the *df* spectrum (steeper *f*-curve) and shift it to higher temperatures while decreasing E_a will broaden the peak and shift it to lower temperatures for a given heating rate (Fig. 2). Holding E_a constant, an increase in diffusivity (D_o/a^2) will narrow the peak and shift it to lower temperatures, while decreasing diffusivity will broaden the

peak and shift it to higher temperatures (Fig. 2). Grain size and heating rate also shift release curves, where smaller grains and faster heating rate lead to earlier He release, and vice versa for larger grains and slower heating schedules. In net, the interplay of these variables will modify the locations and shapes of *f*-curves and *df* spectra. Also, since *df* spectra must conserve an area equal to 1, the heights of release peaks will vary depending on the breadth of the peak and presence of any complexities in ^{4}He release or secondary He components, i.e. those components outside normal VD expectations (Fig. 1).

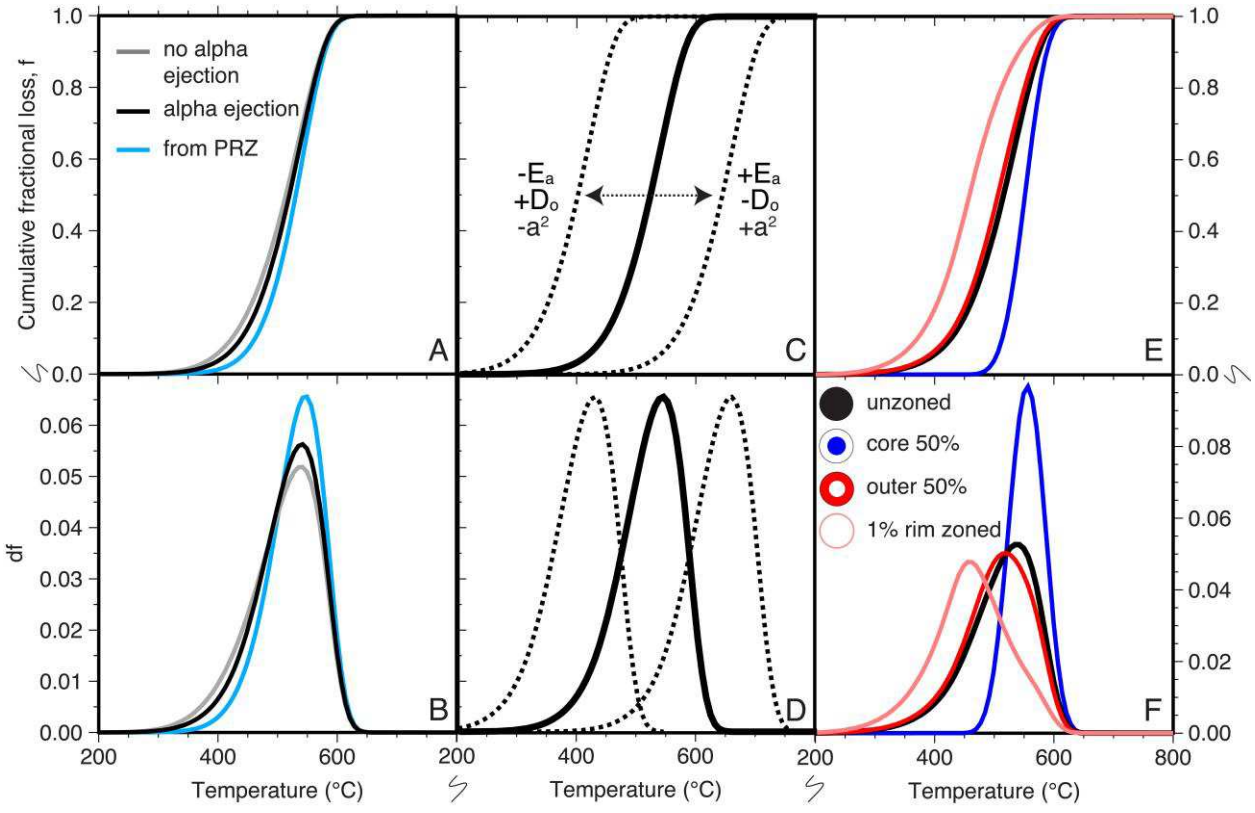

Figure 2. Cumulative fractional loss (*f*-curve) derived from Crank-Nicolson 1D implicit finite-difference diffusion models, using spherical geometry for a 100 µm radius apatite under simulated laboratory conditions of 20°C/minute heating rate (21.5 s time step) and Durango apatite diffusion kinetics (E_a = 138 kJ/mol (33 kcal/mol) and ln D_o/a^2 = 13 m^2/s (D_o of 50 cm^2/s); Farley (2000)). (A) Curves illustrate the difference between cases of no-alpha ejection, alpha ejection, and a grain from the apatite partial retention zone (PRZ) that cooled from 80° to 60°C. A case was also simulated for slow cooling (0.5°C/Ma) with alpha ejection but was nearly indistinguishable from the quenched grain with alpha ejection (black curve). (B) Corresponding *df* spectra showing impact of no/alpha ejection and PRZ cases. (C) Variation in grain size (diffusion domain, a^2), heating rate, or changes to diffusivity (D_o) and activation energy (E_a) can shift the cumulative release curve in loss-temperature space, (D) the same effects on the *df* spectrum peak. (E) The effects of U-Th zoning on the *f*-curve, and (F) the same zoning effects on *df* spectra.

To constrain some possible behaviors that might be observed due just to volume diffusion, we modeled several extreme scenarios using a 1D Crank-Nicolson finite-difference solution. These models consider the effects of heterogeneous alpha-ejection, cooling rate, and parent distribution on concentration profiles and their outgassing in cumulative loss-curve form (Fig. 2). Models were run for unzoned grains with and without alpha ejection, and for three extreme cases where all ^{4}He was located in the inner 50% of the spherical radius, the outer 50% of the spherical radius, and the outer 1% of the spherical radius. The cumulative fractional loss curves (Fig. 2A) reflect the presence of non-flat concentration profiles as minor shifts in curve form, as is also true for *df* spectra (Fig. 2B). Modeling the effects of parent-isotope zoning in instantaneously-cooled grains (Fig. 2E-F) shows modest variability in peak shape and location between unzoned and outer-zoned examples, with deflection of the peak top to cooler temperatures. The core-zoning example is markedly different, with a steep, narrow peak shifted to higher temperatures due to delayed diffusional loss. The main outcomes to note are that zoned samples should still display only smooth, unimodal behavior during outgassing, and that release-peak details are sensitive only to fairly extreme zoning.

It is important to clarify nomenclature we use throughout this paper to describe the ^{4}He components released during CRH analysis. Taking a thermochronological viewpoint, we refer to the "radiogenic" component as gas that is released during heating as expected by volume diffusion assuming typical apatite kinetics, and the "extraneous" component as ^{4}He that falls outside of theoretical expectations for diffusion. This is mainly expressed as a separate or distinct component present at high temperatures (see below, and Fig. 1). Our categorization of CRH results into an *expected* group are mainly based on those grains that release ^{4}He following simple VD behavior with an obvious single radiogenic component (i.e. Durango apatite) whereas *anomalous* results are grains where there are multiple gas components or release behavior not typified by VD.

The closed-system behavior that is expected in traditional geochronology is focused on the radiogenic gas that is completely retained in a mineral since its formation. This is different in thermochronologic scenarios that involve closure and partial open-system behavior, since some of the *in situ* radiogenic ^{4}He production is not expected to be retained. If such ^{4}He were to

become trapped, this component is excess with respect to thermochronologic expectations but from another perspective still radiogenic in its origins. As an example, as discussed below and in Zeitler et al. (2017), in a slowly-cooled setting it may be possible that radiogenic He that would normally diffuse out of an apatite crystal at higher temperatures instead would be trapped in crystal voids, mechanical defects, or high radiation-damage zones, leading to a situation where the crystal "self-pollutes" and yields an older than anticipated (U-Th)/He age. This situation would hypothetically yield CRH results that resemble an expected VD component of gas plus a secondary, extraneous component that is characterized by higher activation energy or retarded diffusivity.

2.4 Peak fitting and age correction

To quantify the magnitude of the extraneous components present in some of our samples, we began by using a VD model based on the simple Arrhenius relationship. The observed *df* spectra from apatite unknowns were fitted to a VD model by using the sample's actual grain radius and then allowing activation energy, diffusion coefficient, and the *df* spectrum amplitude to vary. For the purpose of isolating components using peak fitting of small portions of the *df* spectrum, our goal was merely to define a function of the proper form expected for temperature-activated diffusion, rather than extract accurate kinetic information from the sample. This approach was necessary because real samples in the laboratory outgas at a broader range of higher temperatures than predicted by simple VD, due to the well-known deviation from linear Arrhenius behavior observed in apatite at temperatures above 280-325°C (Farley, 2000; Shuster et al., 2006).

In cases of complex release behavior, the fitted volume-diffusion curve was used to remove superfluous portions of the ^{4}He signal taking the form of spikes or late-released gas, as follows. The observed *df* spectra were first smoothed using a 12-point median filter to remove any discrete gas-release spikes, after which the volume-diffusion model was fit to the lower-temperature release data. Honoring as much of the lower-temperature observed data as possible, the final corrected He content was taken to be the sum of the integral across the observed fitted data, plus the integral across the extrapolated VD model at those higher temperatures beyond which there was deviation from simple, smooth behavior (see Fig. 1). Generally, when comparing unknowns to the VD model, apparent activation energies required for good fits were

commonly ~109 kJ/mol (~26 kcal/mol), lower than the accepted values for Durango apatite due to the Arrhenius non-linearity discussed above. For this first attempt at correcting for extraneous components, because we lacked a simple model for what causes delayed gas release, we did not attempt any peak-stripping analysis in regions where components overlapped.

In determining CRH-corrected ages, we first propagated all analytical uncertainties from He, U, Th, and Sm measurements and those associated with the F_T (alpha-loss) and blank correction for conventional (U-Th)/He age calculation. To estimate the uncertainties on CRH corrections, a range of plausible extraneous-gas corrections was determined using model activation energy bounds of ~109 and ~146 kJ/mol (25 and 35 kcal/mol) to approximate typical and extreme end-member conditions, and the standard deviation of these corrections was then convolved with our conventional error estimation. The added 1σ uncertainty is typically on the order of ~2-5% for CRH age corrections, but it can be higher (>10%) for curves that are more difficult to correct (e.g., those with ambiguous peaks or very noisy *df* signals). At this point in our understanding, the uncertainties inherent in performing CRH corrections are difficult to systematize because *df* spectra are unique for each grain. Rigorous error estimation associated with CRH age correction is an issue clearly requiring more study, but is beyond the scope of this paper.

2.5 Samples

We performed CRH experiments on single crystals from various sample suites for which we had previous analytical data and knowledge of age dispersion and geological context. It is important to note that we chose samples from a range of environments showing a range of behaviors. The data we present are not necessarily representative of any one "typical" sample suite, geological environment, or of apatites in general.

We report data from apatites obtained from slowly-cooled rocks (≤1°C/Ma) from central Mongolia, the central Appalachian Mountains in Pennsylvania, and the Sierra Nevada; rapidly-cooled rocks (~10°C/Ma) from Tibet; and quenched volcanic rocks, (Durango and Mt. Dromedary apatites) (Table 1). We also examined two apatite samples that had been soaked with high He partial pressures as a part of a study of He solubility (Zeitler et al., 2017).

Table 1: Natural apatite sample suites

Sample Provenance	Host rock	Cooling Rate (°C/Ma)	Typical eU (ppm)	Exp. U-Th/He Age (Ma)	Obs. Age Range (Ma)
MN: Hangay Mtns. Mongolia	granite/diorite	~0.3-0.5	< 10-135 30 (avg)	122.7 ± 24.0 (2σ)	~80-220
APL: Appalachians PA, USA	granite	~0.4	< 10-25	164.1 ± 5.1 & 183.2 ± 7.4 (2σ)	~85-245
R/SN: Sierra Nevada, CA	granodiorite	~0.8-1.3	~65 (avg)	~40-50	~35-90
MDC: Mt. Dromedary, AUS	monzonite	~1.5-2	~62 (avg)	86.6 (mean)*	77.8-100.8
NB: Namche Barwa, Tibet	gneiss	~10-15	~10-40	~2-8	~10-200
DUR: Durango, Mexico	rhyolite tuff	>10	~60 (avg)	31.44 ± 0.18 (2σ)	–

Table 1. Natural apatite samples examined in this paper. References for sample groups: Hangay, Mongolia: McDannell (2017); Appalachian samples CHFD and SCDM: McKeon et al. (2014); Sierra Nevada: (Fayon and Hansen, 2015); Mt. Dromedary: Persano (2003); Namche Barwa: Zeitler et al. (2014); Durango: McDowell et al. (2005).

2.5.1. Durango, Mexico Age Standard

We used internal fragments (180-250 μm) of the Durango fluorapatite (U-Th)/He age standard (31.44 ± 0.18 Ma, 2σ) obtained from the rapidly cooled volcanics of the Cerro de Mercado mine in Durango City, Mexico (McDowell et al., 2005). Durango apatite is used as an age standard because it is plentiful, is rapidly cooled, and has large cm-scale crystal sizes that allow utilization of internal shards that have not experienced alpha loss. However, Durango is an atypical apatite because of its high effective uranium content (eU = [U+0.235×Th]; Flowers et al. 2009), unusual Th/U, and significant zoning in U and Th, e.g. (Boyce and Hodges, 2005).

2.5.2. Hangay Mountains, Mongolia, Older and Slowly Cooled

The Hangay Mountain apatite samples are from Permo-Triassic granitoids in Mongolia (McDannell, 2017). These rocks comprise a slowly-cooled terrane that has experienced denudation rates over the past ~100 Ma comparable to other ancient settings such as the Appalachians. Cooling rates through the mid-to-late Cretaceous were <1°C/Ma when (U-Th)/He cooling ages were set (McDannell, 2017). Ages are typically ~100 Ma in the Hangay Mountains and slightly older and much more variable in the outlying region. These apatites display a range of eU and grain size. Internal age dispersion is variable between samples, and in the worst cases

replicate ages span 10s of m.y., while other grains replicate within error. The nature of dispersion in this dataset is difficult to assess, mainly due to the large sampling area.

2.5.3. Namche Barwa, Tibet, Younger, More Quickly Cooled

Zeitler et al. (2014) presented apatite (U-Th)/He data for southeastern Tibet, where basement rocks underwent rapid cooling and exhumation from about 15 to 5 Ma. Apatite data are generally quite well behaved and not dispersed with the exception of several samples: single-grain (U-Th)/He ages for sample NB-07 are ~11, ~14, and ~25 Ma in contrast to numerous nearby samples which yield ages of 7 to 9 Ma; sample NB-54 single-grain ages are ~13, ~56, and ~204 Ma, in contrast to nearby samples which yield ages of ~2-7 Ma. We choose these two samples to investigate a case of extreme dispersion in which the reference ages are well defined.

2.5.4. Sierra Nevada, California Shear Zone

Fayon and Hansen (2015) presented preliminary apatite (U-Th)/He results for grains taken from a small-scale reverse shear zone and from undeformed country rock of the Round Valley Peak granodiorite in the Sierra Nevada of California. There are multiple shear zones (~8) cutting the Round Valley Peak granodiorite between Big McGee Lake and Hopkins Pass, potentially related to emplacement of the Mono Creek granite. Fayon and Hansen (2015) suggested that cooling-age dispersion increases with deformation, and they attributed this to increased dislocation density within the crystal lattice. In their study, deformed sample 1989s24 showed single-grain ages ranging from 36 to 87 Ma with a mean of 57.9 ± 19.5 Ma, whereas the undeformed bedrock apatites yield less dispersed ages between 37 to 42 Ma, with a mean age of 40.4 ± 1.7 Ma.

2.5.5. Appalachian Mountains, Pennsylvania, USA, Older, More Slowly Cooled

McKeon et al. (2014) presented (U-Th)/He data that showed signs of problematic behavior from slowly-cooled terranes of the Appalachian Mountains in the eastern USA. Scattered (U-Th)/He results from other studies of Appalachian samples are common and well documented, (e.g. Littlefield, 2010; Spotila et al., 2004; Taylor and Fitzgerald, 2011). Physical and chemical abrasion of Appalachian grains suggests that some are afflicted by severe crystal-core U-Th zonation, contributing to dispersed cooling ages (McKeon, 2012). Further detailed LA-ICPMS 3D grain mapping showed that these apatites exhibit significant and complex U-Th zonation

(Fox et al., 2014). Previous analyses of grains APL-CHFD-00 and APL-SCDM-00 yield age ranges of 156 to 372 Ma and 176 to 191 Ma, respectively (McKeon et al., 2014). The McKeon et al. (2014) apatites are from granitic rocks and sample CHFD has low, pooled eU <10 ppm, while the eU for sample SCDM is 26 ppm, which is about the typical apatite value. Under typical Appalachian cooling rates of 0.4°C/Ma, CHFD apatites experienced closure near ~50°C, however SCDM apatite closure would be offset about 12°C warmer under slow cooling conditions due to radiation-damage effects. This difference in closure temperature equates to some 30 Ma of increased age for SCDM grains, consistent with the difference in minimum ages reported.

2.5.6. Mt. Dromedary, Australia, Rifted Margin

Rocks of the Mount Dromedary Complex were emplaced during opening of the Tasman Sea in the Cretaceous and are now exposed along the southeastern Great Escarpment margin of Australia (Ollier, 1982). The region underwent cooling rates on the order of ~1.5 to 2°C/Ma through the apatite He partial retention zone, resulting in apatite (U-Th)/He ages from the region that are 80 to 120 Ma (Persano, 2003; Persano et al., 2005). Thermal histories suggest that for some samples Cretaceous cooling was slightly more rapid, with samples to some degree being exhumed from within the He partial retention zone. The sample we examined, GA1550, is from the same location as the biotite K-Ar and $^{40}Ar/^{39}Ar$ age standard (98.5 ± 0.5 Ma; McDougall and Wellman, 2011), and the same general locale as the Mt. Dromedary apatite fission-track age standard (98.7 ± 1.1 Ma; Green, 1985). Dromedary apatite (U-Th)/He ages typically range between ~80-90 Ma, and nearby to the southwest, apatite cooling ages range between 78 to 101 Ma, with an average of ~86 Ma (Persano, 2003; Persano et al., 2005). The cooling rates near Mt. Dromedary equate to closure temperatures of ~68-69°C using the RDAAM model (Flowers et al., 2009), while conventional Durango kinetics yield a closure temperature ~10°C lower.

2.5.7. Solubility Samples, Soaked at High He Partial Pressures

We also examined two samples from a study of He solubility in apatite reported by Zeitler et al. (2017). One sample consisted of grains of Durango apatite standard that had been pre-annealed of irradiation damage and then soaked at 31 bars of ^{4}He partial pressure at 650˚C for over 1364 hours. The other sample (NC/SY2a,b) was a slowly cooled apatite from the southern

Appalachians (McKeon et al., 2014); this was soaked at 12.2 bars of ^{4}He partial pressure at 647˚C for 1853 hours, but was not pre-annealed. Zeitler et al. (2017) found that these samples showed an extremely wide range of apparent ^{4}He apparent solubilities with values reaching as high as 4e-8 mol/g. Based on the assumption that the lowest measured values provide estimates for true ^{4}He solubility, for the Durango sample the expected ^{4}He content due to solubility is 7.1e-10 mol/g, and for NC/SY2a,b, ~3e-10 mol/g.

3. Results

In total, we examined 135 single apatite grains using CRH analysis, and saw outcomes ranging from nearly ideal outgassing curves to those that were highly anomalous with respect to simple diffusion behavior (Fig. 3). Anomalous behavior included sharp spikes in gas release, usually at low to moderate temperatures, and extended gas release at higher temperatures, often though not always manifesting as a second fairly distinct gas-release peak.

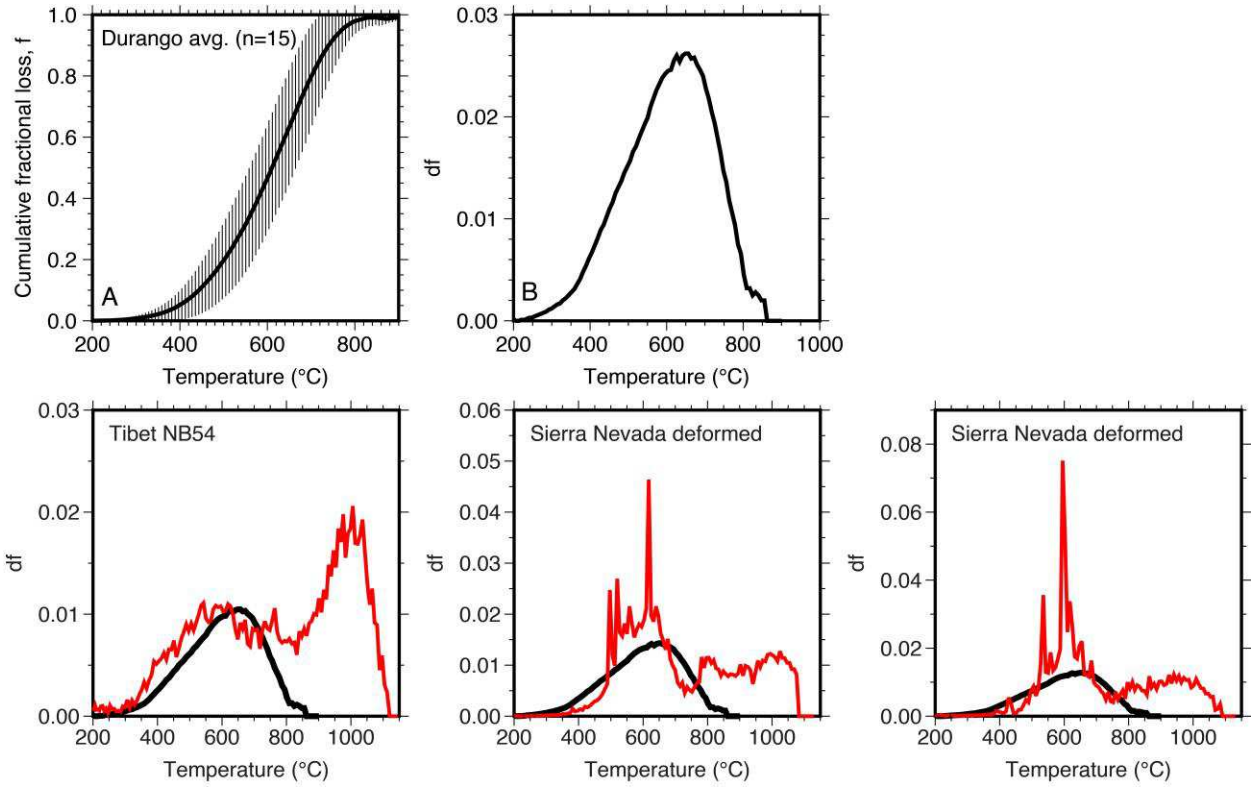

Figure 3. Upper panels: (A) Plot of the mean cumulative *f* with increasing temperature following a 20°C/min heating rate for Durango apatite (n=15) shown with two standard deviations. (B) Average *df* spectrum for the same grains as in panel A. Durango apatites obey smooth, simple diffusive behavior.

Analyzed internal shards are 180-250 μm, with a spherical equivalent radius (R_s) of ~100 μm. Note: The subtle irregularities seen in late Durango release are averaging artifacts due to temperature variability for complete grain outgassing. Lower panels: Three examples of anomalous *df* spectra (red), compared to the average Durango spectrum (black). Note that the Durango spectra were rescaled in each example to more closely overlap the lower-temperature release of the companion curve. The anomalous samples are characterized by the presence of significant He released as higher temperatures and also spikes of released He, most frequently seen at lower to moderate temperatures. Note that anomalous spectra do show a lower-temperature component of He release coincident with the radiogenic He release shown by Durango samples.

As an aid in discussion we divide the 122 natural samples we investigated using the CRH method into three semi-quantitative categories, (1) expected, (2) intermediate, and (3) anomalous, based on diffusive behavior during outgassing. Apatite grains showing *expected* behavior release between ~5% to 95% of their ^{4}He between ~450 to 800°C and are totally exhausted by ~900°C (using our heating protocol), as is observed in the degassing behavior of a reference group of Durango standard grains (Fig. 3). Apatite grains we designated as *anomalous* showed some combination of distinct inflections in *f*-curves (represented as multi-modal *df* spectrum), significant gas spikes, or other severe deviation from smooth release, while apatite grains we designated as *intermediate* showed some minor irregularities in *df* spectra or minor shifts in outgassing temperature relative to Durango. In cases where small spikes or "tails" amounting to only a few percent or less of the total He are present in *df* spectra, grains were characterized as *intermediate* even though they were not completely consistent with simple diffusive behavior.

Below, we briefly review the results from the various sample suites. The Mongolian sample suite is a dataset from a landscape evolution study involving regional sampling from rocks that have undergone slow cooling, whereas the other suites, mainly the Tibetan and Sierra Nevada samples were chosen explicitly because of their previously known age scatter for testing and applying the CRH method. Complete CRH analytical data for each grain can be found in the supplement data repository Table DR1 and individual sample suite results can be found in Tables DR2 to DR6.

3.1 Results from individual sample suites

3.1.1 Mongolia

Mongolian examples make up the majority of our CRH screening results and this suite is our closest approximation of a typical (U-Th)/He sample set. They displayed a range of behaviors (Fig. 4) extending from simple smooth release to the presence of gas spikes and/or an anomalously retentive He component. Out of the 53 grains analyzed using normal selection criteria, 13 show expected behavior, 14 show intermediate behavior, and 26 show anomalous behavior. One inclusion-filled grain from sample 12MN22 was purposely selected for analysis and showed distinctly anomalous behavior (Fig. 4).

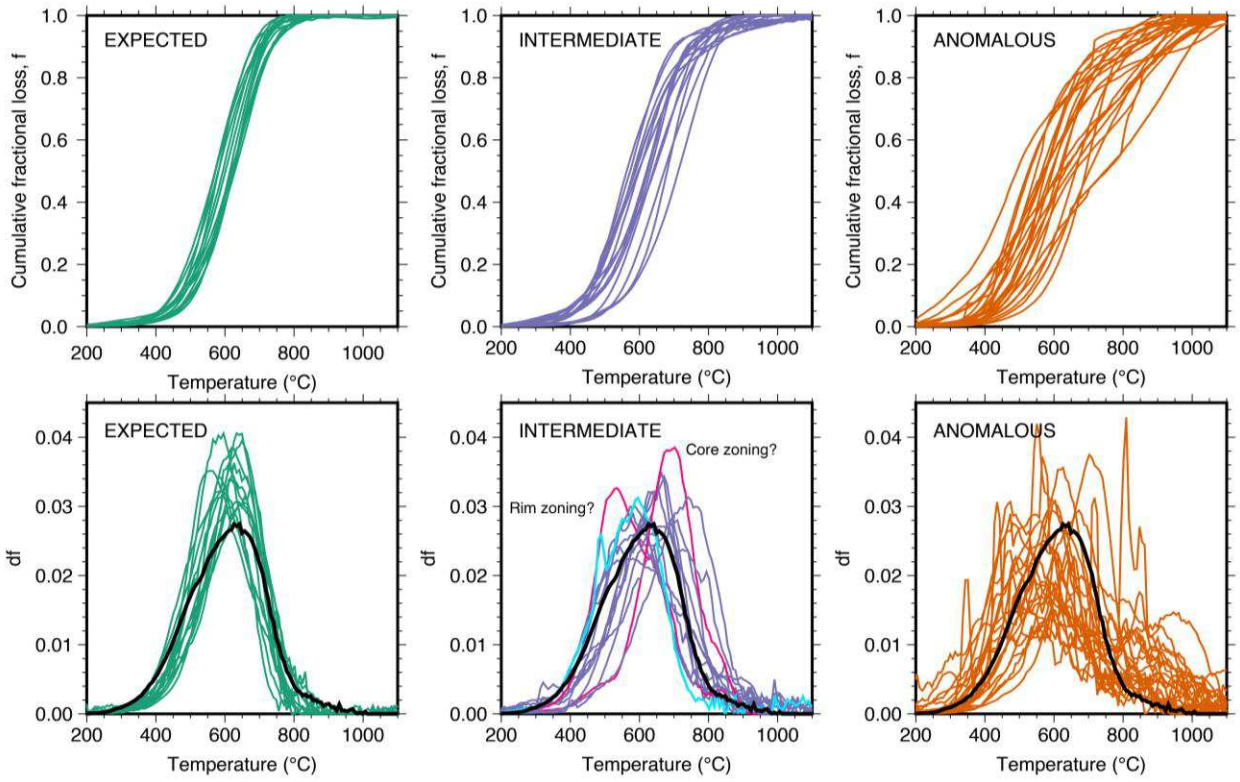

Figure 4: Summary of *f*-curves and *df* spectra from Mongolian samples. In these examples the grains that follow smooth expected behavior in green are tightly grouped and *df*-curves are very similar to a representative Durango curve shown in black. The intermediate group shows more variability in release behavior and in the case of the two samples (red curves) appear to first-order to match the isotopic-zoning models for core and rim zoning (Fig. 2F). Sample 12MN22 is shown in blue. The anomalous group shows non-smooth release with many gas spikes and deferred release beyond what is typically expected. In each case, plotted *df* spectra are smoothed using a 3-point moving average.

3.1.2 Southeastern Tibet

Apatite samples NB-07-26 and NB-54 from southeastern Tibet have a well-established thermochronological context and were selected because they show significant age dispersion.

During CRH analysis, most grains from both samples showed very anomalous behavior involving both discrete release spikes and a significant component of He released at high temperatures (Fig. 5).

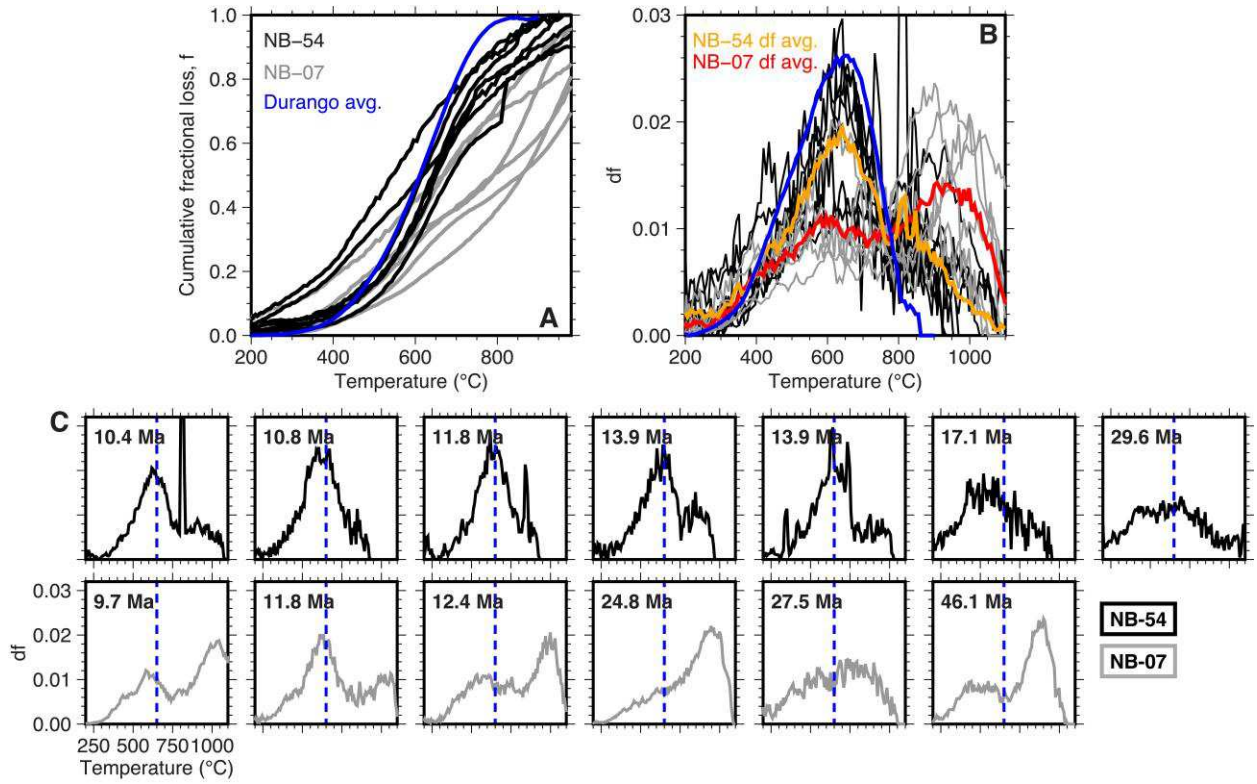

Figure 5. (A) Cumulative fractional loss and smoothed (3 pt. moving average) *df* spectra for Tibetan samples NB-07-26 (gray) and NB-54 (black). (B) NB-07 displays a substantial gas component delayed to high-temperature; red spectrum gives average for all grains. NB-54 looks much better overall; compare its average (orange) to the Durango average (blue), but has elevated early release and minor higher-temperature gas release as well. Most of these grains (mainly NB-07) never quite reached 100% ^{4}He loss, even above 1100°C. Because He signals for these young samples are low their *df* spectra are noisy, but significant gas-release spikes can still be seen. (C) Individual CRH *df* spectra for NB-54 (black) and NB-07 (gray) with respective conventional (U-Th)/He age for each apatite arranged in ascending order; only grains that were dated (rounded ages) are shown. Blue dashed line shows typical location of Durango *df* spectrum peak. See supplement for all data.

3.1.3 Sierra Nevada

This sample suite allows a comparison of CRH results from apatite from an undeformed granodiorite sample (R9515) and a nearby sample from a shear zone in the granodiorite (1989s24) for which conventional analyses show significant dispersion. Apatite grains from the relatively undeformed sample fall broadly into our “intermediate” category, showing behavior

fairly similar to the average Durango apatite, with generally smooth release and almost total degassing by about 900°C, although there appears to be a small amount (<5%) of gas released at higher temperatures (Fig. 6B). In contrast, apatites from the shear zone deviate markedly from smooth diffusive behavior (Fig. 6C) and their *df* spectra reveal a spurious high-temperature tail representing ~40% of the total gas released. Apatites from both samples in some cases show release spikes, though in the deformed sample these are far more numerous and often overlapping.

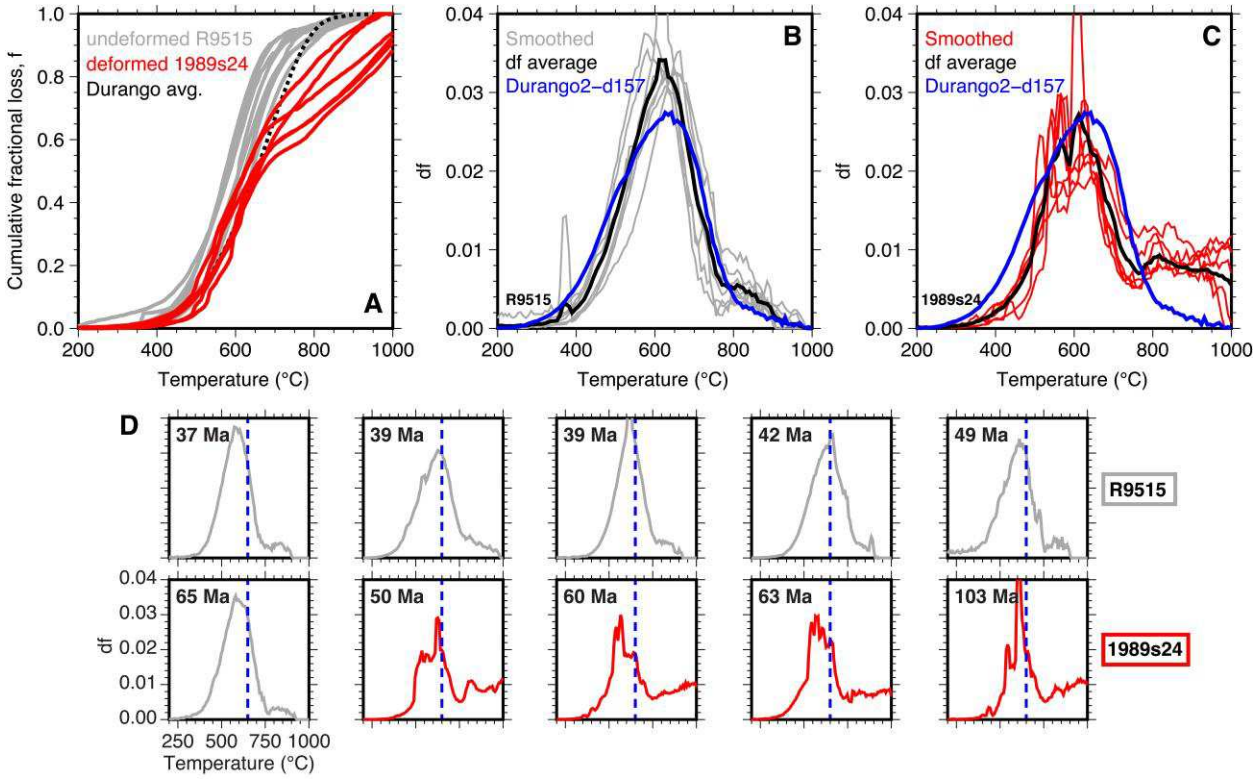

Figure 6. Screening results for two samples from the Round Valley Peak granodiorite in the Sierra Nevada: the relatively undeformed R9515, and the deformed apatite, 1989s24, where the latter shows considerable age scatter, originally reported by Fayon and Hansen (2015). (A) Cumulative *f*-loss with increasing temperature for multiple R9515 samples (gray lines) and sample 1989s24 (red lines). Here R9515 is relatively well-behaved. Black dashed line is the *f*-loss of an averaged bundle of 15 Durango apatites. (B) Smoothed (3 pt. moving average) *df* spectra for R9515 in gray, while the black line shows the average behavior of the group. A typical Durango is shown for comparison (blue spectrum) and the R9515 'intermediate/expected' group is similar in behavior to the Durango example. (C) Same as B but for the deformed sample 1989s24, where there is an irregular, narrow peak shape and clearly a high-temperature component that deviates from both smooth, expected behavior and Durango behavior. (D) Individual *df* spectra for undeformed and deformed grains with their respective conventional (U-Th)/He ages; only grains that were dated (rounded ages) are shown. Blue dashed line shows typical location of Durango *df* spectrum peak. See supplement for all data.

3.1.4 Appalachians

The Appalachian samples APL-CHFD-00 and APL-SCDM-00 are from another old, slowly-cooled region, one that showed considerable dispersion for some samples (McKeon et al., 2014). While generally well-behaved (Fig. 7), we characterize these grains as intermediate in their outgassing behavior because in addition to some release spikes and small higher-temperature tails, the samples release gas at distinctly higher temperatures compared to the average Durango apatite and the average of the well-behaved Mongolian apatites (Fig. 4). The *df* spectra for most grains also show peaks that are wider at their tops when compared to other samples.

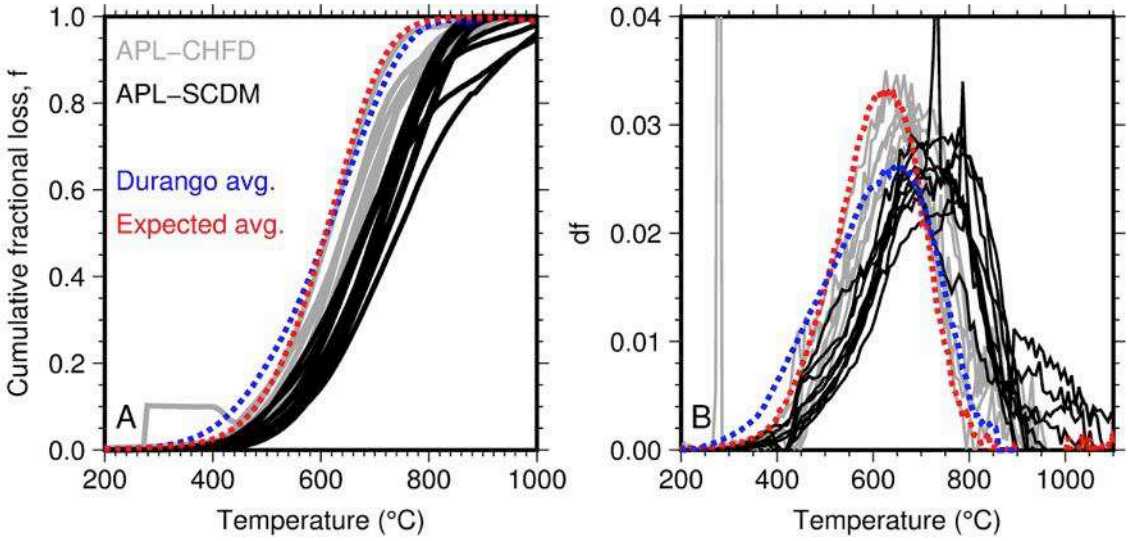

Figure 7. Screening results for Appalachian apatites from SE Pennsylvania. Cumulative *f*-curves are offset to higher temperatures compared to Mongolian subset observing expected behavior (dashed red curve, n=6) and Durango average (dashed blue curve, n=15), with sample APL-CHFD being more delayed and still releasing He at temps. >1000°C. If APL grains were kinetically the same as Durango or expected examples they should approximately overlap. APL spherical equivalent radii are ~70-100 μm, smaller or roughly equal to Durango fragments, therefore a shift to higher temperatures is unlikely to be related to grain size, however higher eU is a common characteristic of the more retentive grains.

3.1.5 Mt. Dromedary

Mt. Dromedary Complex apatites represent another slowly cooled region, albeit one that may have experienced some slightly more rapid exhumation from within a He partial retention zone than other presented datasets. ^{4}He release from the majority of grains is offset to higher temperature (Fig. 8), similar to the Appalachian grains (Fig. 7).

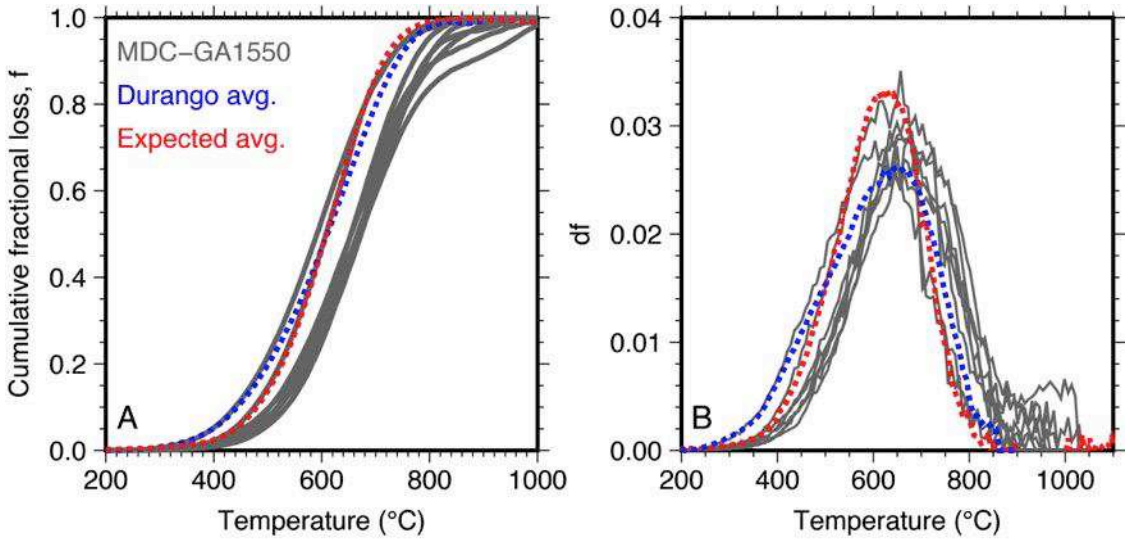

Figure 8. Cumulative fractional loss and *df* spectra for Mt. Dromedary grains (GA-1550). Note the relatively consistent behavior with release deferred to higher temperature. Two apatites are clearly offset from the rest of the group and align well with an expected group of Mongolian samples (red curve) and the Durango average (blue curve).

3.1.6 Solubility study samples

The apatites from these two samples are different than all the other natural samples in that they should contain no radiogenic ^{4}He, with all their He having been acquired during laboratory treatment. Zeitler et al. (2017) argued that while a small part of the He uptake was related to solution into normal lattice sites, most of the gas was taken up by crystal imperfections of some sort, possibly microvoids. Notably, grains from these samples released significant percentages of their He content when mechanically crushed under vacuum.

Figure 9 shows CRH analysis of 12 individual grains from these samples. There is a strong correlation between total He content and complexity of CRH gas release. Samples having gas contents close to predictions for Henry's Law solubility show smooth simple *df* spectra identical to Durango, whereas samples with gas contents far in excess of solubility show more irregular gas release substantially deferred to higher temperatures.

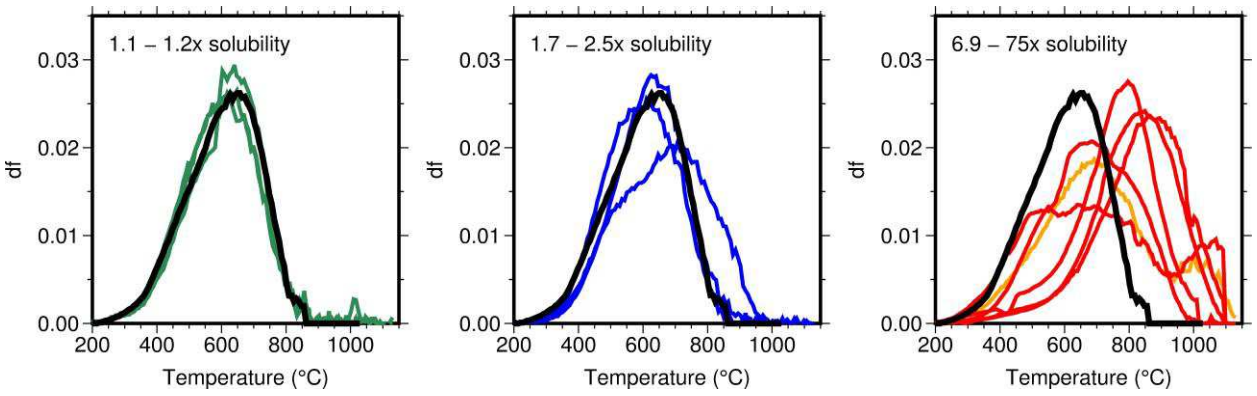

Figure 9. *df* spectra for solubility samples, arranged by total He content relative to predictions of a solubility model. Black curve is for Durango average. The orange curve at right is for a grain with a relative content of 6.9X; results shown in red range are for grains with relative He contents between 16.5X and 75X.

3.3 Summary of CRH Results

If the expected and intermediate results are grouped together then of the 122 natural grains we assessed, about half demonstrate fairly smooth diffusive behavior and the other half exhibited clearly anomalous outgassing characteristics (Fig. 10). It is important to keep in mind that his overall assessment does not apply to apatite He diffusion behavior in general, since our results reflect our choice of samples. Omitting results from the Sierra Nevada and Tibetan samples, which were chosen to examine specific cases of known dispersion, about 35% of all grains (from the Mongolian, Appalachian, and Mount Dromedary samples) are characterized by anomalous gas release.

There is an apparent relationship between (U-Th)/He age and anomalous behavior that is most discernible in the Tibetan and Sierra Nevada apatites (Figs. 5 and 6) and the solubility examples (Fig. 9). The relationship in the other sample suites are less obvious, but given our results there are a variety of recognized characteristics that could potentially be sources of anomalous CRH behavior, including fluid-inclusion decrepitation causing gas spikes and microvoids that host either purely radiogenic or retained autogenic ^{4}He that should have been diffused out of the grain at higher temperatures. Below we explore the use of a potential age correction scheme for anomalous samples and further discuss characteristics of aberrant gas release.

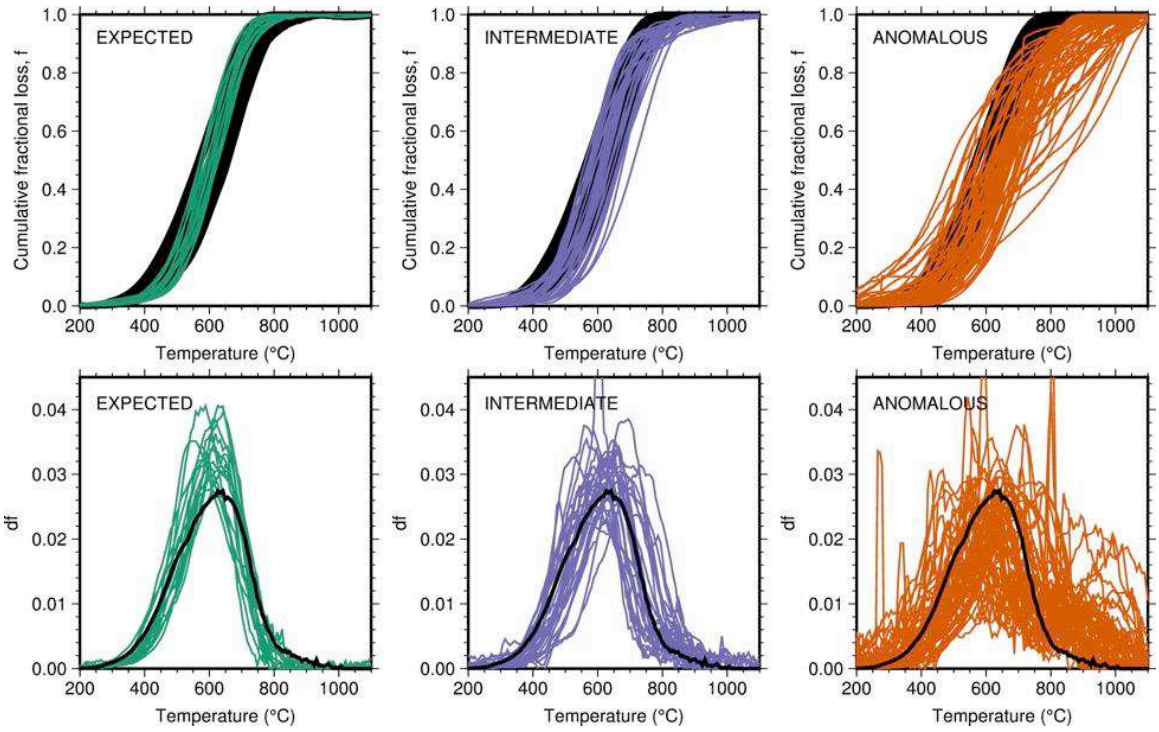

549

550 **Figure 10.** Summary of the CRH (U-Th)/He screening results for the natural apatite suites shown in
551 Table 1, separate into expected, intermediate, and anomalous groupings. Black envelope (upper plots)
552 represents 16 Durango apatites (180-250 µm sieve size) for comparison. Cumulative *f*-curves suggest
553 'expected' grains are completely outgassed by ~900°C, while intermediate examples show more flattened
554 release at high-temperature due to unusually strongly retained He, but are nonetheless exhausted by ~950-
555 1000°C. Anomalous grains have a less sigmoidal, and sometimes linear approach to high-temperature and
556 some are still outgassing past 1000°C. *df*-curves (bottom plots) smoothed using a 3-pt. moving average.
557 Black spectrum is Durango apatite, for reference.
558

559 **3.4 Age Correction Based on CRH Results**

560 Given that CRH analysis can reveal the presence of both gas-release spikes as well as anomalous
561 high-temperature release, we explored the degree to which it might be possible to correct (U-
562 Th)/He ages by removing these extraneous gas components in order to isolate the purely
563 radiogenic ^{4}He content expected to be retained during normal closure. As we noted earlier
564 (Section 2.4), this is not a simple process and rigorous assessment of uncertainty is not yet
565 possible. For instance, since we do not yet have a model for what is controlling higher-
566 temperature release, it is not possible to know the degree to which release of radiogenic He by
567 normal diffusion overlaps with the higher-temperature release, or if part of the ^{4}He released at
568 high-temperatures is in fact part of the expected radiogenic "closure" component but is liberated
569 late due to more retentive siting within voids or defects within a grain. In the case of spikes,

570 correction is simple except when multiple closely spaced spikes coalesce into an elevated
571 shoulder. The ideal case of truly separate gas components, in terms of siting and diffusive
572 behavior, should result in age correction that is effective at reducing dispersion. Alternatively, if
573 mixing of multiple gas components occurs during ^{4}He release then CRH correction may be less
574 effective in reducing age dispersion. For all of these reasons the age corrections we propose
575 should be viewed as an exploratory attempt to see if age correction has promise.
576
577 Figure 11 shows various aspects of the peak-fitting and age-correction process. These examples
578 were chosen to show particular issues, but it is important to note that for a number of
579 complicated samples (e.g., see Fig. 3), objective peak-fitting is difficult. Peak-fitting was done
580 on all samples that required it, given our fitting criteria, but only a few examples are shown here
581 for brevity. Tables DR2-DR6 provide analytical information for age determinations and age
582 corrections.
583
584 The Mongolian CRH examples in Figure 11C-F the observed *df* spectra are shown with VD
585 model predictions that were fit to sections or the entire observed data curve. In cases where gas
586 spikes and/or high-temperature "excess" gas were present, fitting necessitated the removal of
587 these components (shown by gray line as 'fit section'). Grain 14MN09-d157 (Fig. 11C) is an
588 example of the 12-point median filter that was used to smooth *df*-curves and the VD model
589 correction was applied to the peak shoulder to remove excess He. This grain has a conventional
590 (U-Th)/He age of 109.87 ± 1.63 Ma and a >15% reduction in age following CRH correction
591 (91.6 ± 1.8 Ma).
592
593 Sample 12MN22 (Fig. 11D) has a conventional single grain He age of 190.41 ± 3.35 Ma and one
594 grain (12MN22-d158) degassed using the CRH method yields a total-gas age of 227.10 ± 4.87
595 Ma (before CRH correction), with similar grain size and eU between both grains. If the gas spike
596 and slight high-temperature irregularities are removed from the *df*-curve, the CRH single-grain
597 He age recalculates to 204.7 ± 4.5 Ma. The difference in arithmetic mean between conventional
598 (U-Th)/He and CRH corrected ages produces a ~5% mean age reduction and shows better
599 internal age consistency. This apatite is an example of a purposely degassed grain with

inclusions, while a third grain from this sample that contained visible inclusions was also purposely degassed using conventional single-step heating and gave a much older age >300 Ma.

Sample 12MN36A (Fig. 11E) generally exhibits smooth release, and was dated using both conventional (U-Th)/He analysis (n=2) and CRH analysis (n=4). This sample does display slight eU-age correlation and no clear trend in grain size with age is observed. The grain shown in the figure corrects from 98.87 ± 1.41 Ma to ~83 Ma when the small gas "tail" is removed. Conventional ages for this sample range from ~96-130 Ma with a mean of 111.97 ± 1.5 Ma, and after CRH correction the mean is 108.61 ± 1.5 Ma.

In cases where irregular behavior was observed, such as in Figure 11F, the VD model was fit to the entire observed *df*-curve. For sample 14MN18, conventional (U-Th)/He cooling age replicates yielded dates of ~139, ~145, ~211 without CRH correction, and these replicates display slight grain size-age correlation but approximately the same eU between each grain (single-grain age in Fig. 11F is 211.29 ± 3.28). The two younger ages for sample 14MN18 demonstrate expected behavior (not shown), while the ~211 Ma grain shown here deviates from smooth release between ~400-600°C and corrects to 172.6 ± 10.4 Ma. This grain is ~35% larger than the other grains, so a result older than the average grains is expected. In all 14MN18 cases, the level of correction is moderate and where there is greater scatter it can usually be explained by grain size or eU.

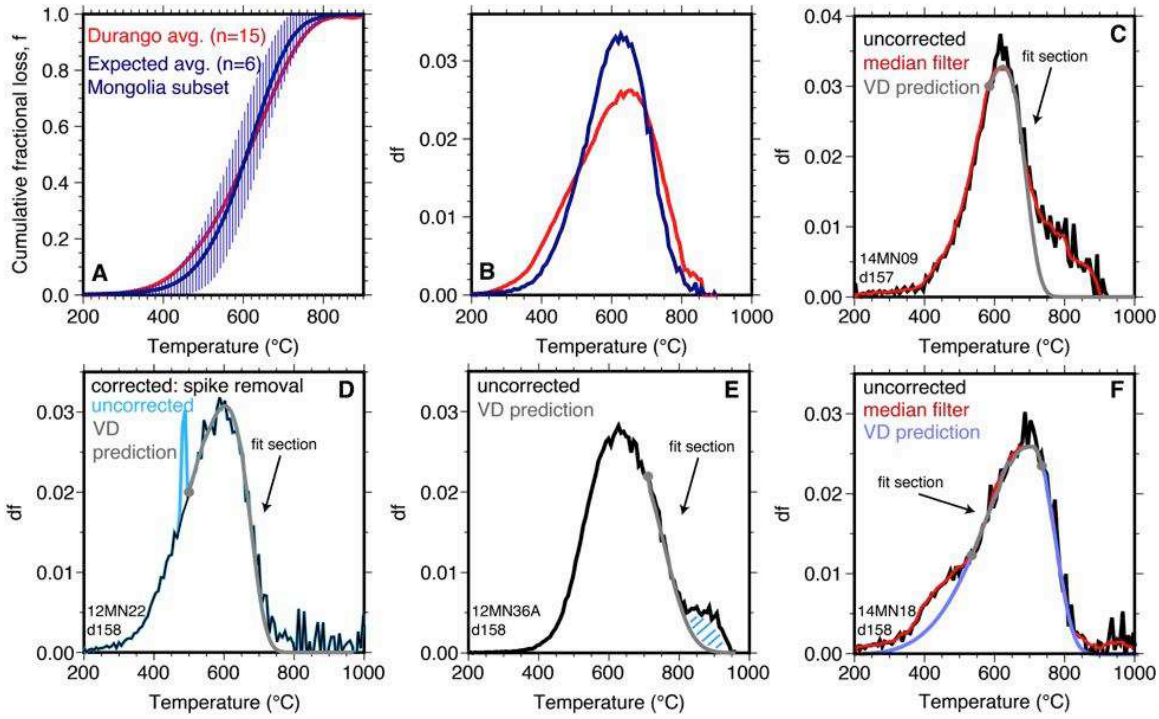

Figure 11. Overview of peak fitting and age correction**.** (A) Subset of Mongolian apatites (mean ± 2 standard deviation of fractional loss values) that show "expected" smooth behavior similar to the Durango average. The difference between the two curves could in part be explained by the internal-shard Durango grains not having any alpha-ejection depletion, i.e. expressed as delay in release from He-poor outer grain edge (see Fig. 2). (B) Difference in *df* spectra between the Mongolian and Durango group averages. No age correction would be applied for these samples. Panels C-F: Examples of peak fitting applied to various Mongolian apatite *df* spectra in order to obtain a CRH-corrected age. Examples of He-content correction: (C and E) removal of minor to moderate high-temperature shoulder; (D) manual gas-spike removal; (D and F), removal of minor gas component released above ~850°C; (E), honoring observed data until the shoulder, after which extrapolations of the diffusion model is used; and (F), fitted diffusion model used entirely in place of observed data.

Figure 12 summarizes age corrections made using CRH analysis for all *df* spectra we felt could be modeled. In some cases, the age reductions associated with stripping anomalous He components reduce dispersion and also move mean results much closer to known or geologically reasonable results (e.g., Tibet and possibly the Sierra Nevada samples). In other cases, however, while age correction lowers extreme ages, it also appears to over-correct younger ages, such that total dispersion is not significantly reduced. To be consistent, all grains were corrected regardless of categorization to show that grains that follow *expected* behavior generally have a very small age reduction compared to those that are *anomalous*.

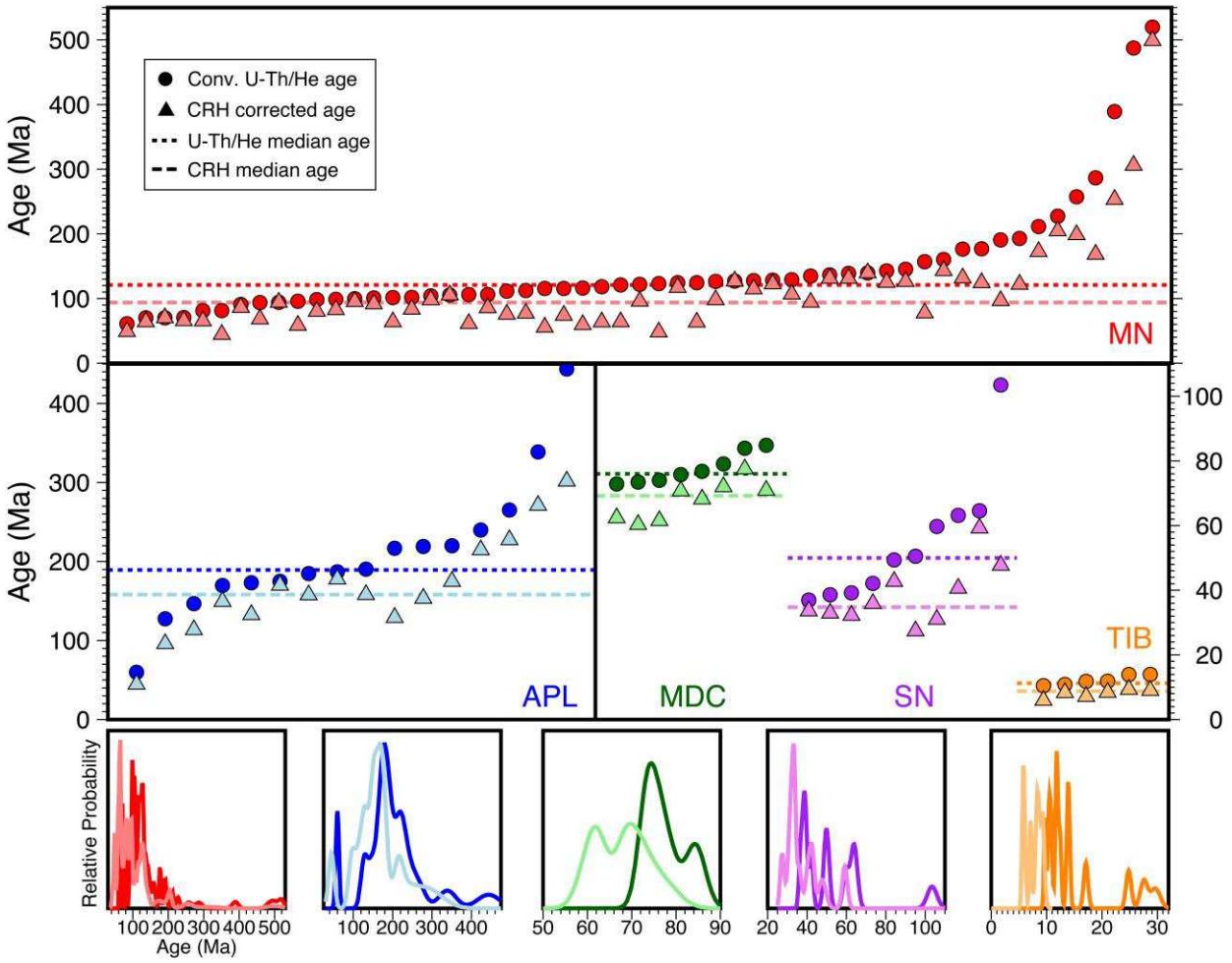

643

644 **Figure 12.** Ranked results organized by sample suite, showing uncorrected conventional (U-Th)/He ages
645 (circles) and corrected ages (triangles) using the CRH method. Dashed lines indicate the median for
646 uncorrected and corrected data from each sample suite. The median was calculated using the entire
647 population of each suite, disregarding individual sample replicates to assess overall change. Only ages
648 that could be corrected are shown; see supplementary data table DR1 for individual ages and errors.
649 Notice change in y-axes. (Bottom) Age probability density plots show the change in age distributions
650 before and after correction. MN = Mongolia; APL = Appalachian; MDC = Mt. Dromedary Complex; SN
651 = Sierra Nevada; TIB = Tibet.
652

653 **4. Discussion**

654 Our CRH analyses reveal information about the systematics of He outgassing from apatite. One
655 clear result is that many samples – about half, though admittedly including many replicates of
656 Durango apatite – showed fairly simple behavior consistent with volume diffusion. On the other
657 hand, complex behavior was more common than we had anticipated, given that most of the
658 grains we analyzed were carefully selected. Overall, we would argue that CRH analysis lives up

to its promise of providing insight into He-diffusion systematics and is an easy and fairly rapid means of screening samples early in the analytical process. We also argue that at this stage in our understanding, samples showing anomalous release behavior under CRH analysis should be culled from data sets before age determinations are made, since such anomalous behavior is inconsistent with the diffusion theory that forms the basis for obtaining thermal history information. We propose that it is far better to use CRH analysis to avoid contaminating data sets with such problematic results, rather than measuring conventional ages and then being left with a dispersed and hard-to-explain set of ages.

Below, we discuss a number of observations that bear on these conclusions.

4.1 Kinetic variability and sensitivity of the method

As predicted by models (Fig. 2), CRH analysis appears able to detect differences in kinetic properties and even He distribution. For instance, there is a subtle but consistent difference in the shapes of *f*-curves and *df* spectra between whole-grain samples and internal shards of Durango apatite (e.g., Figure 11A,B). This likely reflects the relatively homogenous distribution of radiogenic He in Durango compared to the discrete grains, which will have alpha-ejection and in many cases diffusion profiles along their outer margins. Moreover, in a few cases, *df* spectra, though smooth and simple in form, were clearly skewed in shape, consistent with predictions about the impacts of significant zoning on release spectra (e.g. Fig. 4).

In terms of kinetics, most samples show a lower-temperature peak in gas release that for grains of similar size closely overlay with results from Durango apatite (e.g. Figs. 4, 5, 6B). However, the MDC and APL apatites display gas release that is consistently displaced to slightly higher temperatures (Figs. 7, 8). The grain size for the APL samples are approximately equal to or less than our Durango shards, so grain size alone cannot explain the shift to higher temperature. However, eU for the APL grains is consistently higher, implying radiation-damage control of diffusivity (Shuster et al., 2006) (Tables 1 and DR1). This suggests that the CRH approach is capable of identifying this greater retentivity. If more accurate and precise laser heating is used, it should be possible to quantify this change in retentivity by direct measurement of the sample's kinetic parameters (Idleman et al., 2017).

690

691 **4.2 Gas-release components**

692 All *df* spectra including anomalous apatite samples show low- to mid-temperature release of a
693 component of radiogenic He that is consistent with simple volume-diffusion behavior (Fig. 10).
694 Added to this component, the grains we classified as having anomalous degassing behavior
695 display a component whose release was delayed until significantly higher temperatures,
696 sometimes in the form of a second *df* peak and other times as an extended interval of gas release.
697

698 In a number of cases, anomalous samples also showed gas spikes, varying in number and usually
699 occurring at low to medium temperatures, below ~800˚C. We speculate that the sharp spikes in
700 gas release are related to decrepitation of fluid-inclusions, as seen in the results from apatite
701 12MN22, which is an apatite purposely chosen because it contained numerous visible inclusions
702 (Fig. 11D), and in many of the apatites from the Sierra Nevada samples (Fig. 6). Given the sharp
703 nature of many of these spikes, we would argue that they must be sourced from inclusions
704 located close to grain margins, with the temperature of decrepitation depending on fluid-
705 inclusion size. It is noteworthy that the solubility samples showed no spikes in gas release
706 (Figure 9), possibly because they were heated to ~650˚C during He soaking, thus decrepitating
707 any larger inclusions or healing crystallographic defects. There is also a possibility that grain
708 fracturing during heating that could release a pulse of He from the newly exposed grain interior,
709 inducing a CRH gas spike.
710

711 The higher-temperature gas release could be explained in several ways. Very small inclusions of
712 more retentive U- and Th-bearing minerals like zircon or xenotime might lead to high-
713 temperature He release. However, this mechanism cannot explain the relatively large amounts of
714 high-temperature He released in some samples, even accounting for higher eU in the inclusions,
715 since the total volume of such inclusions would have been sufficiently small to avoid optical
716 detection, or conversely below the detection limit but volumetrically significant. Alternatively,
717 volume imperfections that have trapped He could act as the source for secondary gas components
718 liberated at high temperatures. This is likely the explanation for the high-temperature release
719 from the solubility samples, most of which were Durango apatite grains unlikely to contain
720 mineral inclusions.

721

722 Trapping in defects also provides an explanation for the Sierra Nevada results, and supports the
723 hypothesis of Fayon and Hansen (2015) that structural damage produces crystal dislocations that
724 can trap He or impede its diffusion. Recent work by Gerin et al. (2017) also documents the He-
725 trapping properties of deformation-induced point defects. The difference between relatively
726 deformed and undeformed samples is very apparent in the cumulative loss curves, with increased
727 deformation leading to more anomalous behavior and a larger secondary gas component at high
728 temperature. Hypothetically, the high-temperature gas component could be radiogenic ^{4}He that
729 has been trapped either syn- or post-cooling, in which case this He would be part of the expected
730 component of retained He. Alternatively, self-contamination through trapping of pre-cooling
731 radiogenic He could occur; this would amount to a violation of the assumption that at
732 temperatures above the closure interval grains act as open systems. Crystallographic voids or
733 defects could yield distinct CRH behavior due to the higher activation energy requirements to
734 liberate He from those sites, similar to the ideas proposed by Shuster et al., 2006, or
735 alternatively, release post-cooling radiogenic gas from high radiation-damaged zones during
736 laboratory heating. Although the results of our attempt at age correction were mixed, our
737 impression is that more often than not, secondary gas-release peaks are more consistent with a
738 model of enhanced retention of pre-cooling radiogenic production.
739

740 It is tempting to conclude that the low- to mid-temperature gas release (usually in the form of a
741 discrete peak in the *df* spectrum) represents radiogenic He produced *in situ*, or in the case of the
742 solubility samples, He that has entered "normal" sites in the apatite lattice. The age-correction
743 results for the Sierra Nevada and Tibetan samples support this idea, as ages calculated using just
744 the low-temperature release converge to more geologically reasonable ages with much less
745 dispersion (see Figure 12).
746

747 Separate from kinetic questions about the conditions under which various components are
748 released are questions about the source of He components of non-radiogenic origin. In the case
749 of mineral inclusions, this is straightforward. For mechanisms involving trapping, three
750 possibilities exist (Zeitler et al., 2017). First, the He could be trapped as a component in fluid
751 inclusions. This He could be released as spikes from inclusions located near the grain surface, or

752 if inclusions are sufficiently small, be injected into the lattice only later during heating. A second
753 possibility is that transient high partial pressures of He could lead to some becoming
754 anomalously trapped, analogous to what happened in the soaking experiments reported by Zeitler
755 et al. (2017). However, it is not known if sufficiently high local partial pressure could develop in
756 nature, and nor are there data about how such He might be incorporated under geological rather
757 than laboratory conditions.
758
759 **4.3 Age correction using CRH analysis**
760 From our reconnaissance-level results, it is not yet clear whether CRH age correction will prove
761 to be a useful procedure suitable for routine application. Age correction seemed to work
762 reasonably well for the younger, more quickly cooled samples in our study (Tibet and Sierra
763 Nevada), but for the others, age correction did not lower age dispersion and in some cases
764 seemed to over-correct ages to values that are too young. Considering the uniform correction
765 treatment for all grains, some examples (e.g. the MDC suite) suggest the over-correction may be
766 related in part to the higher 35 kcal/mol E_a modeling bound being too aggressive when used as a
767 criterion for high-temperature gas component removal. That said, for these examples there are
768 clearly defined constraints on what ages should be expected, and given the relatively small
769 sample populations, we cannot usefully address the roles that grain composition, size, and eU
770 might also be playing. The crucial question about CRH age correction is whether or not apatites
771 release extraneous and radiogenic He over discrete temperature intervals. If they do, even if
772 release of these components overlaps, it should be possible to develop means of isolating the
773 various components. However, it is also possible that features responsible for anomalous
774 behavior alter the release behavior of radiogenic He, such that some of it is released at high
775 temperatures – this would be one explanation for why some ages were overcorrected.
776
777 **4.4 Support for the re-extract protocol**
778 During conventional apatite (U-Th)/He analyses some laboratories perform He re-extracts on
779 apatite grains, where after initial heating the sample is heated again under the same temperature
780 conditions or to even higher temperature to ensure that the grain is fully outgassed, e.g. (Wolf et
781 al., 1996). If the second reheat produces significant ^{4}He (>1-1.5% of He blank), then this is taken
782 as a sign of anomalous behavior and is either noted during reporting or the data are simply

783 considered unreliable due to unidentified mineral inclusions and discarded, e.g. (Farley, 2002).
784 Hot blank re-extraction is crudely analogous to CRH assessment, and based on preliminary
785 assessment of several "bad actor" grains. Idleman et al. (2017) pointed out that the anomalous
786 gas release identified by CRH analysis lends support to the practice of using re-extracts to look
787 for non-ideal behavior in apatites, provided temperatures of heating and re-extraction are
788 accurately controlled. Our experience with our sample set verifies this suggestion, although it is
789 important to note that re-extract analysis cannot identify samples that yield extraneous He in the
790 form of low- to mid-temperature spikes.
791
792 **4.5 Future directions**
793 We would recommend that future screening by CRH be done using optical heating, ideally with
794 a laser, to reach adequate temperatures required for CRH analysis. The benefits of this would be
795 many, including reduction of hydrogen impacts on sensitivity and far better temperature control
796 that would allow accurate diffusion kinetics to be determined for each apatite grain in a short,
797 ~45 minute heating experiment.
798
799 A key next step will be to systematically investigate mechanisms and origins of anomalous
800 release for very well characterized apatite suites in which the expected age is well known and the
801 impacts of mineral and fluid inclusions can be fully assessed separate from the role of any crystal
802 imperfections. The ideal samples would have well-constrained geological and
803 thermochronological contexts, and numerous intact grains with a wide range of eU and chemical
804 composition. With a sufficiently high number of analyses it should be possible to treat the results
805 in multivariate space and assess whether age correction is viable.
806
807 **5. Conclusions**
808 The CRH method is a simple analytical technique that provides a means to rapidly characterize
809 apatite release behavior. Analyses of the Durango apatite standard and samples having little or
810 no age dispersion show simple gas-release behavior consistent with diffusive loss of their ^{4}He at
811 lower temperatures (samples should be completely exhausted by 900˚C using a 20˚C/minute
812 ramp rate while heating). Examples that show complicated release patterns or degas well beyond
813 these temperatures suggest that confounding factors such as mineral inclusions, fluid-inclusion

decrepitation, and impeding of diffusion by crystallographic defects or voids developed through grain deformation, are likely reservoirs of He and causes of anomalous He release in the laboratory. Our results suggest that about half of apatites analyzed using the CRH method demonstrated expected-to-intermediate behavior, although that is specific to this dataset where characterization of He diffusion behaviors was the principal motivation for sample selection. The value of CRH application to (U-Th)/He dating is not only the ability to use degassing character to distinguish between apatites that obey volume diffusion and those that do not, but also offer insight into the underlying mechanisms that are the root cause of abnormal behavior. Whether this information can be used to correct dispersed age datasets is still unclear but is an important possibility worth pursuing.

Acknowledgements

This research did not receive any specific grant from funding agencies in the public, commercial, or not-for-profit sectors. We would like to thank Kenneth Farley and Peter Reiners for extensive comments that improved the manuscript, and Chris Hall for efficient editorial handling. We thank B. Tikoff and L. Goodwin from the University of Wisconsin, Madison for samples from the Sierra Nevada shear zones; we also thank Peter Reiners and the Arizona Radiogenic Dating Laboratory for providing the preliminary pilot ages for the Sierra Nevada samples.

FIGURE AND TABLE CAPTIONS:

Figure 1. Schematic sigmoidal shape of a smooth cumulative fractional loss (*f*-curve; top left) for expected behavior that is then differentiated to produce a *df* spectrum (top right). Bottom shows the *f*-curve and *df* spectrum for a hypothetical sample showing anomalous behavior, in this case a flattened high-temperature *f*-curve which manifests in the *df* spectrum as a secondary release at the peak shoulder (dashed box). This example would be a candidate for age correction (see section 2.4) where the observed data are honored up to the second minor peak, which is then removed using a peak fit through the lower-temperature data.

Figure 2. Cumulative fractional loss (*f*-curve) derived from Crank-Nicolson 1D implicit finite-difference diffusion models, using spherical geometry for a 100 μm radius apatite under simulated laboratory conditions of 20°C/minute heating rate (21.5 s time step) and Durango apatite diffusion kinetics (E_a = 138 kJ/mol (33 kcal/mol) and ln D_o/a^2 = 13 m^2/s (D_o of 50 cm^2/s); Farley (2000)). (A) Curves illustrate the difference between cases of no-alpha ejection, alpha ejection, and a grain from the apatite partial retention zone (PRZ) that cooled from 80° to 60°C. A case was also simulated for slow cooling (0.5°C/Ma) with alpha ejection but was nearly indistinguishable from the quenched grain with alpha ejection (black curve). (B) Corresponding *df* spectra showing impact of no/alpha ejection and PRZ cases. (C) Variation in grain size (diffusion domain, a^2), heating rate, or changes to diffusivity (D_o) and

activation energy (E_a) can shift the cumulative release curve in loss-temperature space, (D) the same effects on the *df* spectrum peak. (E) The effects of U-Th zoning on the *f*-curve, and (F) the same zoning effects on *df* spectra.

Table 1. Natural apatite samples examined in this paper. References for sample groups: Hangay, Mongolia: McDannell (2017); Appalachian samples CHFD and SCDM: McKeon et al. (2014); Sierra Nevada: (Fayon and Hansen, 2015); Mt. Dromedary: Persano (2003); Namche Barwa: Zeitler et al. (2014); Durango: McDowell et al. (2005).

Figure 3. Upper panels: (A) Plot of the mean cumulative *f* with increasing temperature following a 20°C/min heating rate for Durango apatite (n=15) shown with two standard deviations. (B) Average *df* spectrum for the same grains as in panel A. Durango apatites obey smooth, simple diffusive behavior. Analyzed internal shards are 180-250 μm, with a spherical equivalent radius (R_s) of ~100 μm. Note: The subtle irregularities seen in late Durango release are averaging artifacts due to temperature variability for complete grain outgassing. Lower panels: Three examples of anomalous *df* spectra (red), compared to the average Durango spectrum (black). Note that the Durango spectra were rescaled in each example to more closely overlap the lower-temperature release of the companion curve. The anomalous samples are characterized by the presence of significant He released as higher temperatures and also spikes of released He, most frequently seen at lower to moderate temperatures. Note that anomalous spectra do show a lower-temperature component of He release coincident with the radiogenic He release shown by Durango samples.

Figure 4: Summary of *f*-curves and *df* spectra from Mongolian samples. In these examples the grains that follow smooth expected behavior in green are tightly grouped and *df*-curves are very similar to a representative Durango curve shown in black. The intermediate group shows more variability in release behavior and in the case of the two samples (red curves) appear to first-order to match the isotopic-zoning models for core and rim zoning (Fig. 2F). Sample 12MN22 is shown in blue. The anomalous group shows non-smooth release with many gas spikes and deferred release beyond what is typically expected. In each case, plotted *df* spectra are smoothed using a 3-point moving average.

Figure 5. (A) Cumulative fractional loss and smoothed (3 pt. moving average) *df* spectra for Tibetan samples NB-07-26 (gray) and NB-54 (black). (B) NB-07 displays a substantial gas component delayed to high-temperature; red spectrum gives average for all grains. NB-54 looks much better overall; compare its average (orange) to the Durango average (blue), but has elevated early release and minor higher-temperature gas release as well. Most of these grains (mainly NB-07) never quite reached 100% ^{4}He loss, even above 1100°C. Because He signals for these young samples are low their *df* spectra are noisy, but significant gas-release spikes can still be seen. (C) Individual CRH *df* spectra for NB-54 (black) and NB-07 (gray) with respective conventional (U-Th)/He age for each apatite arranged in ascending order; only grains that were dated (rounded ages) are shown. Blue dashed line shows typical location of Durango *df* spectrum peak. See supplement for all data.

Figure 6. Screening results for two samples from the Round Valley Peak granodiorite in the Sierra Nevada: the relatively undeformed R9515, and the deformed apatite, 1989s24, where the latter shows considerable age scatter, originally reported by Fayon and Hansen (2015). (A) Cumulative *f*-loss with increasing temperature for multiple R9515 samples (gray lines) and sample 1989s24 (red lines). Here R9515 is relatively well-behaved. Black dashed line is the *f*-loss of an averaged bundle of 15 Durango apatites. (B) Smoothed (3 pt. moving average) *df* spectra for R9515 in gray, while the black line shows the average behavior of the group. A typical Durango is shown for comparison (blue spectrum) and the R9515 'intermediate/expected' group is similar in behavior to the Durango example. (C) Same as B but for the deformed sample 1989s24, where there is an irregular, narrow peak shape and clearly a high-

temperature component that deviates from both smooth, expected behavior and Durango behavior. (D) Individual *df* spectra for undeformed and deformed grains with their respective conventional (U-Th)/He ages; only grains that were dated (rounded ages) are shown. Blue dashed line shows typical location of Durango *df* spectrum peak. See supplement for all data.

Figure 7. Screening results for Appalachian apatites from SE Pennsylvania. Cumulative *f*-curves are offset to higher temperatures compared to Mongolian subset observing expected behavior (dashed red curve, n=6) and Durango average (dashed blue curve, n=15), with sample APL-CHFD being more delayed and still releasing He at temps. >1000°C. If APL grains were kinetically the same as Durango or expected examples they should approximately overlap. APL spherical equivalent radii are ~70-100 μm, smaller or roughly equal to Durango fragments, therefore a shift to higher temperatures is unlikely to be related to grain size, however higher eU is a common characteristic of the more retentive grains.

Figure 8. Cumulative fractional loss and *df* spectra for Mt. Dromedary grains (GA-1550). Note the relatively consistent behavior with release deferred to higher temperature. Two apatites are clearly offset from the rest of the group and align well with an expected group of Mongolian samples (red curve) and the Durango average (blue curve).

Figure 9. *df* spectra for solubility samples, arranged by total He content relative to predictions of a solubility model. Black curve is for Durango average. The orange curve at right is for a grain with a relative content of 6.9X; results shown in red range are for grains with relative He contents between 16.5X and 75X.

Figure 10. Summary of the CRH (U-Th)/He screening results for the natural apatite suites shown in Table 1, separate into expected, intermediate, and anomalous groupings. Black envelope (upper plots) represents 16 Durango apatites (180-250 μm sieve size) for comparison. Cumulative *f*-curves suggest 'expected' grains are completely outgassed by ~900°C, while intermediate examples show more flattened release at high-temperature due to unusually strongly retained He, but are nonetheless exhausted by ~950-1000°C. Anomalous grains have a less sigmoidal, and sometimes linear approach to high-temperature and some are still outgassing past 1000°C. *df*-curves (bottom plots) smoothed using a 3-pt. moving average. Black spectrum is Durango apatite, for reference.

Figure 11. Overview of peak fitting and age correction**.** (A) Subset of Mongolian apatites (mean ± 2 standard deviation of fractional loss values) that show "expected" smooth behavior similar to the Durango average. The difference between the two curves could in part be explained by the internal-shard Durango grains not having any alpha-ejection depletion, i.e. expressed as delay in release from He-poor outer grain edge (see Fig. 2). (B) Difference in *df* spectra between the Mongolian and Durango group averages. No age correction would be applied for these samples. Panels C-F: Examples of peak fitting applied to various Mongolian apatite *df* spectra in order to obtain a CRH-corrected age. Examples of He-content correction: (C and E) removal of minor to moderate high-temperature shoulder; (D) manual gas-spike removal; (D and F), removal of minor gas component released above ~850°C; (E), honoring observed data until the shoulder, after which extrapolations of the diffusion model is used; and (F), fitted diffusion model used entirely in place of observed data.

Figure 12. Ranked results organized by sample suite, showing uncorrected conventional (U-Th)/He ages (circles) and corrected ages (triangles) using the CRH method. Dashed lines indicate the median for uncorrected and corrected data from each sample suite. The median was calculated using the entire population of each suite, disregarding individual sample replicates to assess overall change. Only ages that could be corrected are shown; see supplementary data table DR1 for individual ages and errors. Notice change in y-axes. (Bottom) Age probability density plots show the change in age distributions

before and after correction. MN = Mongolia; APL = Appalachian; MDC = Mt. Dromedary Complex; SN = Sierra Nevada; TIB = Tibet.

References

Beucher, R., Brown, R.W., Roper, S., Stuart, F. and Persano, C. (2013) Natural age dispersion arising from the analysis of broken crystals: Part II. Practical application to apatite (U–Th)/He thermochronometry. *Geochimica et Cosmochimica Acta* **120**, 395-416.

Boyce, J. and Hodges, K. (2005) U and Th zoning in Cerro de Mercado (Durango, Mexico) fluorapatite: Insights regarding the impact of recoil redistribution of radiogenic 4 He on (U–Th)/He thermochronology. *Chemical Geology* **219**, 261-274.

Brown, R.W., Beucher, R., Roper, S., Persano, C., Stuart, F. and Fitzgerald, P. (2013) Natural age dispersion arising from the analysis of broken crystals. Part I: Theoretical basis and implications for the apatite (U–Th)/He thermochronometer. *Geochimica et Cosmochimica Acta* **122**, 478-497.

Djimbi, D.M., Gautheron, C., Roques, J., Tassan-Got, L., Gerin, C. and Simoni, E. (2015) Impact of apatite chemical composition on (U-Th)/He thermochronometry: An atomistic point of view. *Geochimica et Cosmochimica Acta* **167**, 162-176.

Farley, K.A. (2000) He diffusion from apatite; general behavior as illustrated by Durango fluorapatite. *Journal of Geophysical Research* **105**, 2903-2914.

Farley, K.A. (2002) (U-Th)/He Dating: Techniques, Calibrations, and Applications. *Reviews in Mineralogy and Geochemistry* **47**, 819-844.

Farley, K.A., Wolf, R.A. and Silver, L.T. (1996) The effects of long alpha-stopping distances on (U-Th)/He ages. *Geochimica et Cosmochimica Acta* **60**, 4223-4229.

Fayon, A.K. and Hansen, L. (2015) Effects of deformation on apatite (U-Th)/He single-grain ages, GSA Annual Meeting. The Geological Society of America, Baltimore, MD, USA, p. 293.

Fitzgerald, P.G., Baldwin, S.L., Webb, L.E. and O'Sullivan, P.B. (2006) Interpretation of (U–Th)/He single grain ages from slowly cooled crustal terranes: A case study from the Transantarctic Mountains of southern Victoria Land. *Chemical Geology* **225**, 91-120.

Flowers, R.M. and Kelley, S.A. (2011) Interpreting data dispersion and "inverted" dates in apatite (U–Th)/He and fission-track datasets: An example from the US midcontinent. *Geochimica et Cosmochimica Acta* **75**, 5169-5186.

Flowers, R.M., Ketcham, R.A., Shuster, D.L. and Farley, K.A. (2009) Apatite (U–Th)/He thermochronometry using a radiation damage accumulation and annealing model. *Geochimica et Cosmochimica Acta* **73**, 2347-2365.

Fox, M., McKeon, R.E. and Shuster, D.L. (2014) Incorporating 3‐D parent nuclide zonation for apatite 4He/3He thermochronometry: An example from the Appalachian Mountains. *Geochemistry, Geophysics, Geosystems* **15**, 4217-4229.

Gerin, C., Gautheron, C., Oliviero, E., Bachelet, C., Djimbi, D.M., Seydoux-Guillaume, A.-M., Tassan-Got, L., Sarda, P., Roques, J. and Garrido, F. (2017) Influence of vacancy damage on He diffusion in apatite, investigated at atomic to mineralogical scales. *Geochimica et Cosmochimica Acta* **197**, 87-103.

Green, P. (1985) Comparison of zeta calibration baselines for fission-track dating of apatite, zircon and sphene. *Chemical Geology: Isotope Geoscience section* **58**, 1-22.

Green, P.F., Crowhurst, P.V., Duddy, I.R., Japsen, P. and Holford, S.P. (2006) Conflicting (U–Th)/He and fission track ages in apatite: enhanced He retention, not anomalous annealing behaviour. *Earth and Planetary Science Letters* **250**, 407-427.

Idleman, B.D. and Zeitler, P.K. (2014) Rapid characterization of noble-gas kinetics using continuous heating and gas accumulation, 14th International Conference on Thermochronology, Chamonix, France.

Idleman, B.D., Zeitler, P.K. and McDannell, K.T. (2017) Characterization of He release from apatite by continuous ramped heating. *Chemical Geology*. doi:10.1016/j.chemgeo.2017.11.019

Lieszkovszky, L., Filippelli, A.R. and Tilford, C.R. (1990) Metrological characteristics of a group of quadrupole partial pressure analyzers. *Journal of Vacuum Science & Technology* **A8**.

Littlefield, K.V. (2010) (U-Th)/He analysis of denudation rates and exhumation histories in southern West Virginia, Geology and Geography. West Virginia University, Morgantown, WV.

McDannell, K.T., Idleman, B.D. and Zeitler, P.K. (2015) Characterization of He diffusion behavior from continuous heating experiments: Sample screening and identification of multiple 4He components, AGU Fall Meeting. American Geophysical Union, San Francisco, CA.

McDannell, K.T. (2017) Methods and application of deep-time thermochronology: Insights from slowly cooled terranes of Mongolia and the North American craton, Earth and Environmental Sciences. Lehigh University, Bethlehem, Pennsylvania, p. 261.

McDougall, I. and Wellman, P. (2011) Calibration of GA1550 biotite standard for K/Ar and 40 Ar/39 Ar dating. *Chemical Geology* **280**, 19-25.

McDowell, F.W., McIntosh, W.C. and Farley, K.A. (2005) A precise 40 Ar–39 Ar reference age for the Durango apatite (U–Th)/He and fission-track dating standard. *Chemical Geology* **214**, 249-263.

McKeon, R.E. (2012) Apatite U-Th/He Thermochronometry in Slowly Eroding Landscapes: Addressing Age Dispersion to Understand Appalachian Topographic Development, Earth and Environmental Sciences. Lehigh University.

McKeon, R.E., Zeitler, P.K., Pazzaglia, F.J., Idleman, B.D. and Enkelmann, E. (2014) Decay of an old orogen: Inferences about Appalachian landscape evolution from low-temperature thermochronology. *Geological Society of America Bulletin* **126**, 31-46.

Murray, K.E., Orme, D.A. and Reiners, P.W. (2014) Effects of U–Th-rich grain boundary phases on apatite He ages. *Chemical Geology* **390**, 135-151.

Ollier, C. (1982) The Great Escarpment of eastern Australia: tectonic and geomorphic significance. *Journal of the Geological Society of Australia* **29**, 13-23.

Persano, C. (2003) A combination of apatite fission track and (U-Th)/He thermochronometers to constrain the escarpment evolution in south eastern Australia: a case study of high elevation passive margins. University of Glasgow.

Persano, C., Stuart, F.M., Bishop, P. and Dempster, T.J. (2005) Deciphering continental breakup in eastern Australia using low-temperature thermochronometers. *Journal of Geophysical Research: Solid Earth* **110**.

Peyton, S.L., Reiners, P.W., Carrapa, B. and DeCelles, P.G. (2012) Low-temperature thermochronology of the northern Rocky Mountains, western USA. *American Journal of Science* **312**, 145-212.

Reiners, P.W. and Nicolescu, S. (2006) Measurement of parent nuclides for (U-Th)/He chronometry by solution sector ICP-MS, *ARHDL Report 3.0 ed.* University of Arizona.

Shuster, D.L., Flowers, R.M. and Farley, K.A. (2006) The influence of natural radiation damage on He diffusion kinetics in apatite. *Earth and Planetary Science Letters* **249**, 148-161.

Spiegel, C., Kohn, B., Belton, D., Berner, Z. and Gleadow, A. (2009) Apatite (U–Th–Sm)/He thermochronology of rapidly cooled samples: The effect of He implantation. *Earth and Planetary Science Letters* **285**, 105-114.

Spotila, J.A., Bank, G.C., Reiners, P.W., Naeser, C.W., Naeser, N.D. and Henika, B.S. (2004) Origin of the Blue Ridge escarpment along the passive margin of Eastern North America. *Basin Research* **16**, 41-63.

Taylor, J.P. and Fitzgerald, P.G. (2011) Low-temperature thermal history and landscape development of the eastern Adirondack Mountains, New York: Constraints from apatite fission-track thermochronology and apatite (U-Th)/He dating. *Geological Society of America Bulletin* **123**, 412-426.

1056 Vermeesch, P., Seward, D., Latkoczy, C., Wipf, M., Günther, D. and Baur, H. (2007) α-Emitting
1057 mineral inclusions in apatite, their effect on (U–Th)/He ages, and how to reduce it.
1058 *Geochimica et Cosmochimica Acta* **71**, 1737-1746.

1059 Warnock, A.C., Zeitler, P.K., Wolf, R.A. and Bergman, S.C. (1997) An evaluation of low-
1060 temperature apatite U-Th/He thermochronometry. *Geochimica et Cosmochimica Acta* **61**,
1061 5371-5377.

1062 Wolf, R.A., Farley, K.A. and Silver, L.T. (1996) He diffusion and low-temperature
1063 thermochronometry of apatite. *Geochimica et Cosmochimica Acta* **60**, 4231-4240.

1064 Zeitler, P.K., Enkelmann, E., Thomas, J.B., Watson, E.B., Ancuta, L.D. and Idleman, B.D.
1065 (2017) Solubility and trapping of He in apatite. *Geochimica et Cosmochimica Acta* **209**,
1066 1-8.

1067 Zeitler, P.K., Herczeg, A.L., McDougall, I. and Honda, M. (1987) U-Th-He dating of apatite: A
1068 potential thermochronometer. *Geochimica et Cosmochimica Acta* **51**, 2865-2868.

1069 Zeitler, P.K., Meltzer, A.S., Brown, L., Kidd, W.S.F., Lim, C. and Enkelmann, E. (2014)
1070 Tectonics and topographic evolution of Namche Barwa and the easternmost Lhasa block,
1071 Tibet. *Geological Society of America Special Papers* **507**.

Table 1: Natural apatite sample suites

Sample Provenance	Host rock	Cooling Rate (°C/Ma)	Typical eU (ppm)
MN: Hangay Mtns. Mongolia	granite/diorite	~0.3-0.5	< 10-135 30 (avg)
APL: Appalachians PA, USA	granite	~0.4	< 10-25
R/SN: Sierra Nevada, CA	granodiorite	~0.8-1.3	~65 (avg)
MDC: Mt. Dromedary, AUS	monzonite	~1.5-2	~62 (avg)
NB: Namche Barwa, Tibet	gneiss	~10-15	~10-40
DUR: Durango, Mexico	rhyolite tuff	>10	~60 (avg)

Figure1

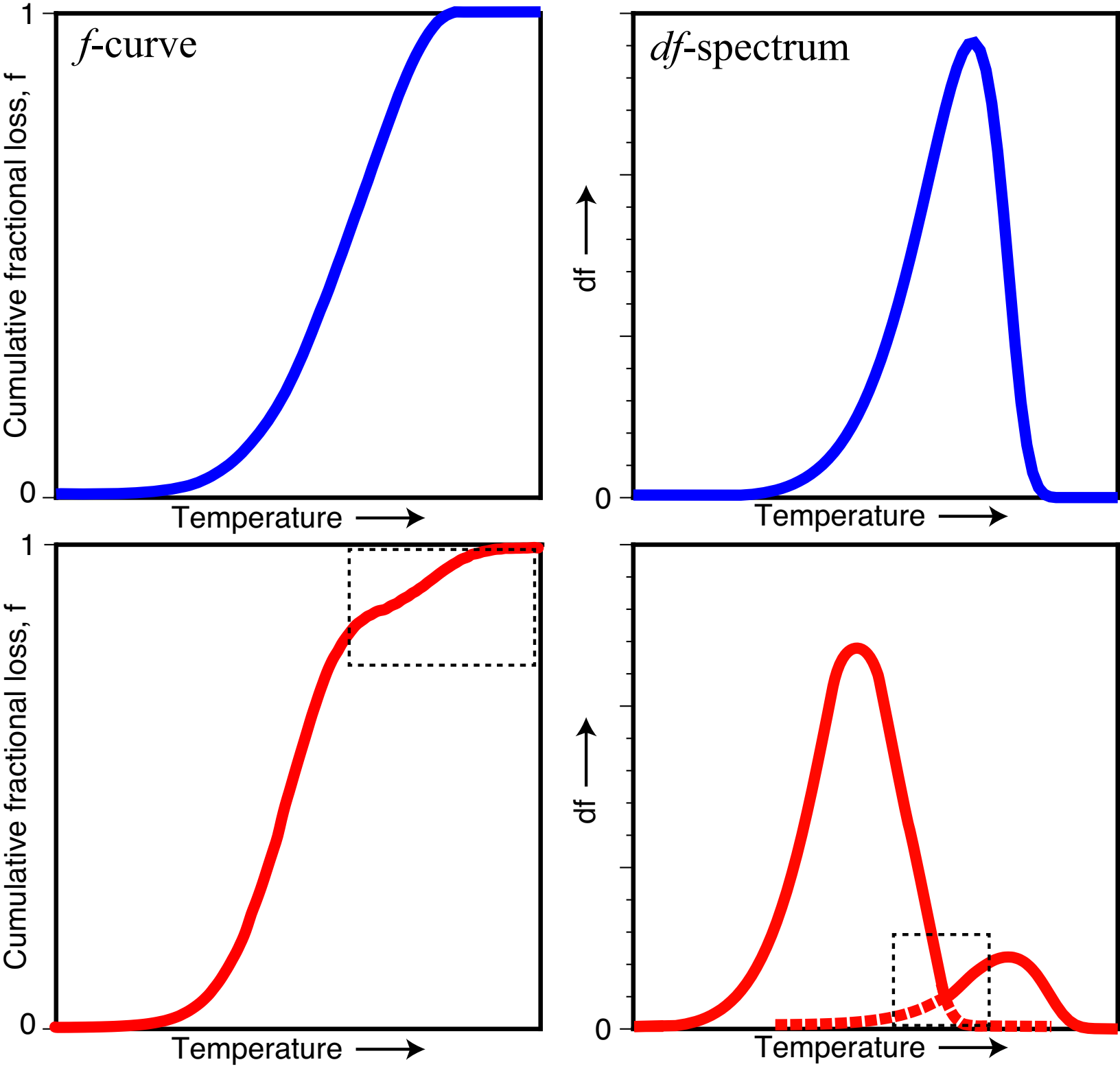
1
f-curve
Cumulative fractional loss, f
0
Temperature
df-spectrum
df
0
Temperature
1
Cumulative fractional loss, f
0
Temperature
df
0
Temperature

Figure2

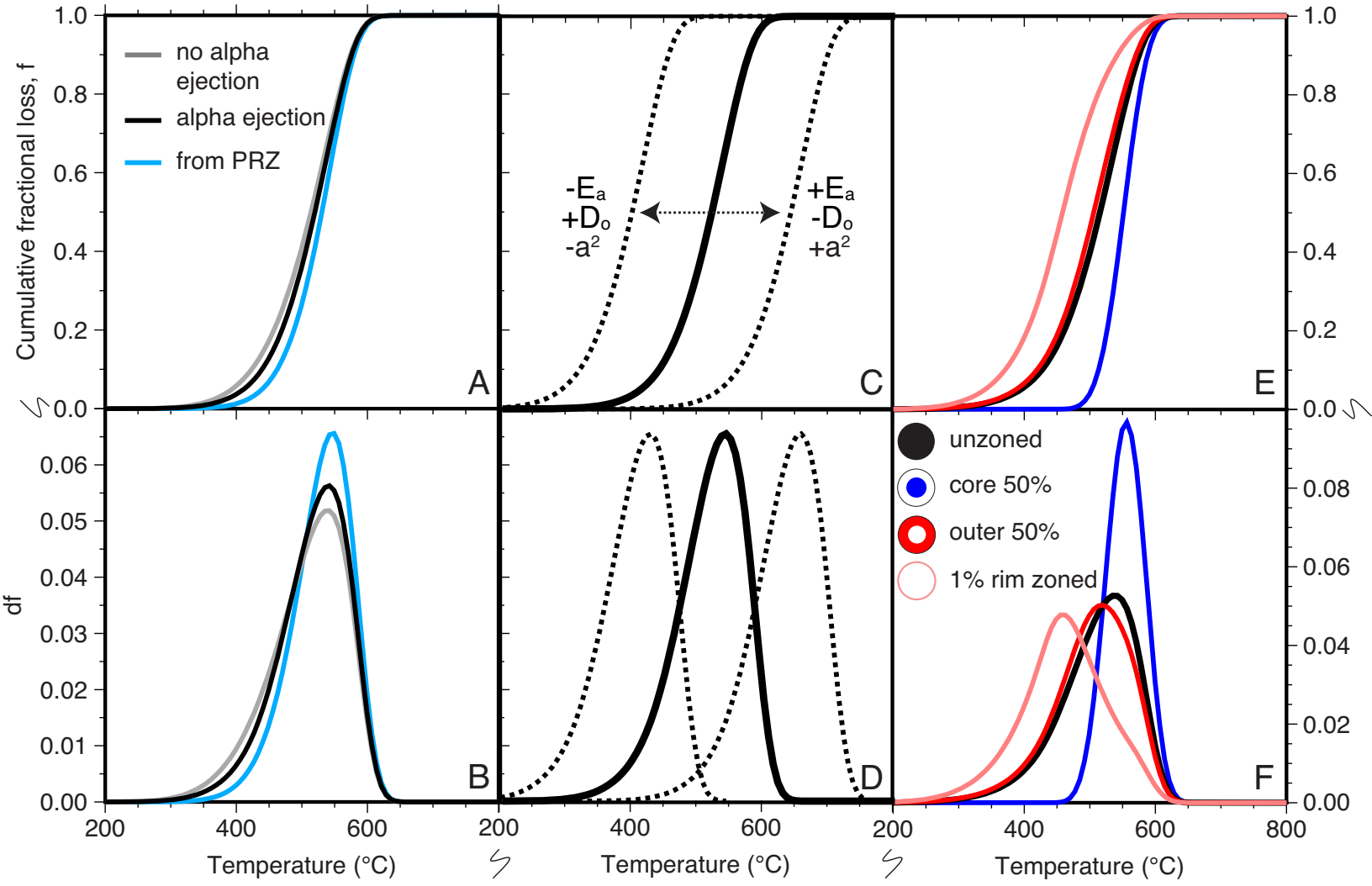
Cumulative fractional loss, f
df
no alpha ejection
alpha ejection
from PRZ
-Ea
+Do
-a2
+Ea
-Do
+a2
unzoned
core 50%
outer 50%
1% rim zoned
A
B
C
D
E
F
Temperature (°C)
Temperature (°C)
Temperature (°C)

Figure3

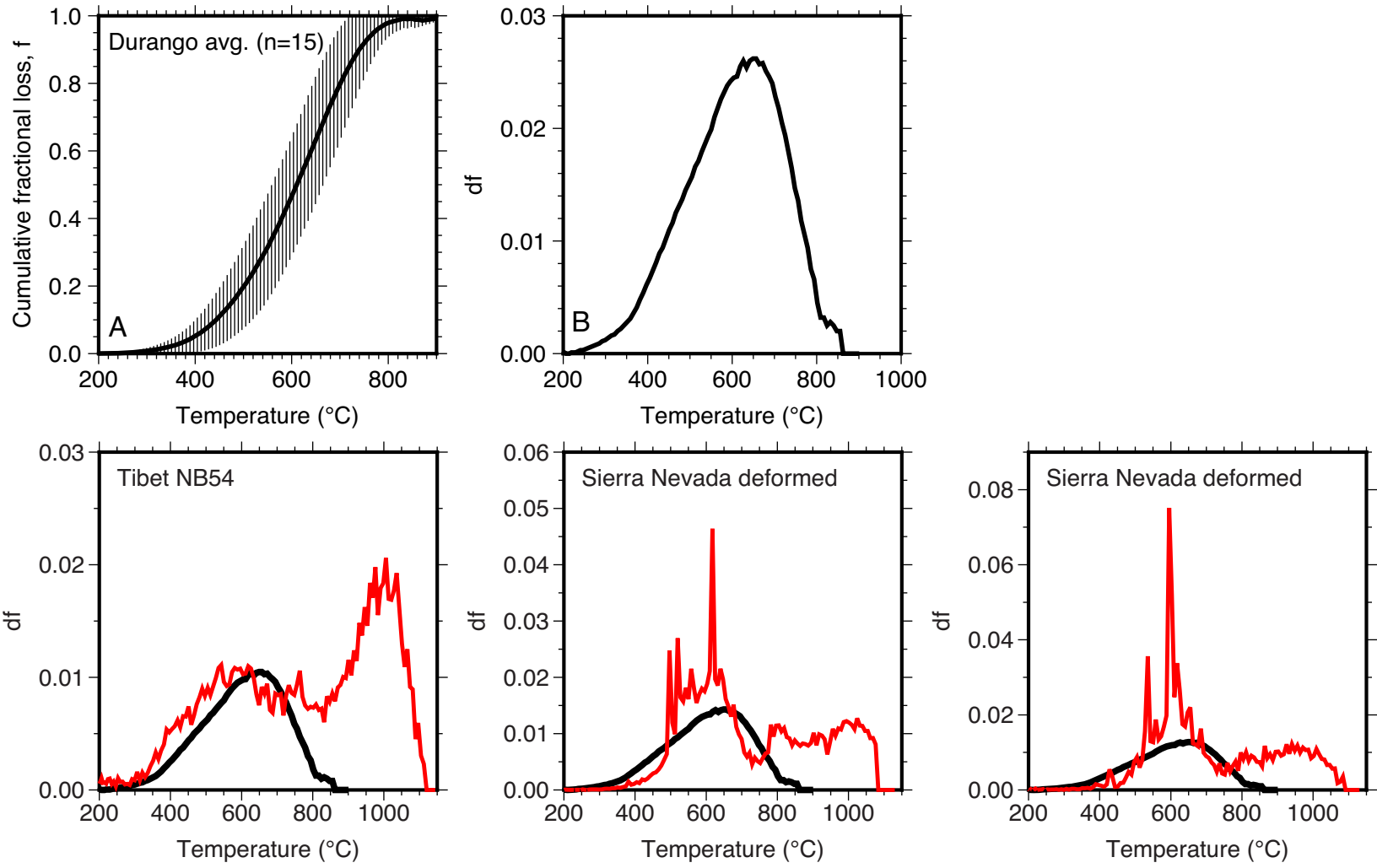
Durango avg. (n=15)
A
Cumulative fractional loss, f
Temperature (°C)
B
df
Tibet NB54
Sierra Nevada deformed
Sierra Nevada deformed

Figure4

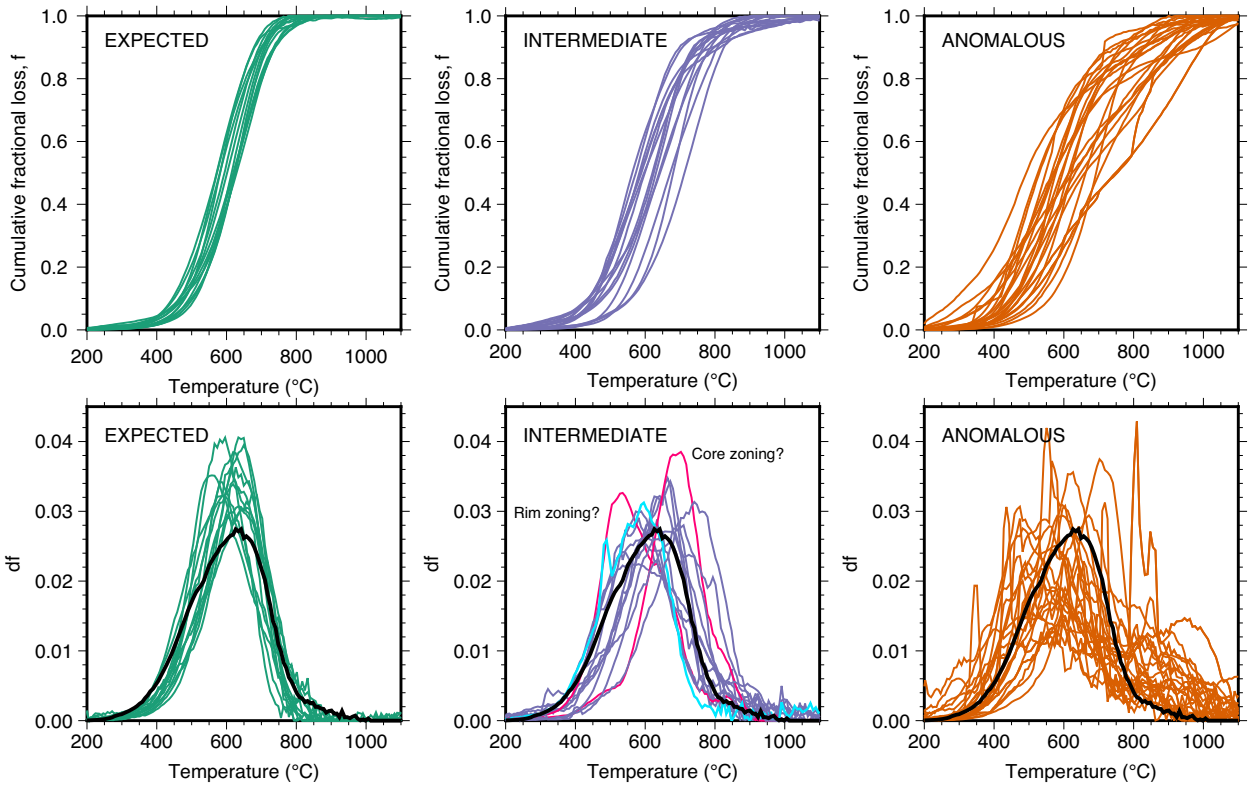
EXPECTED
INTERMEDIATE
ANOMALOUS
Cumulative fractional loss, f
df
Temperature (°C)
Core zoning?
Rim zoning?

Figure5

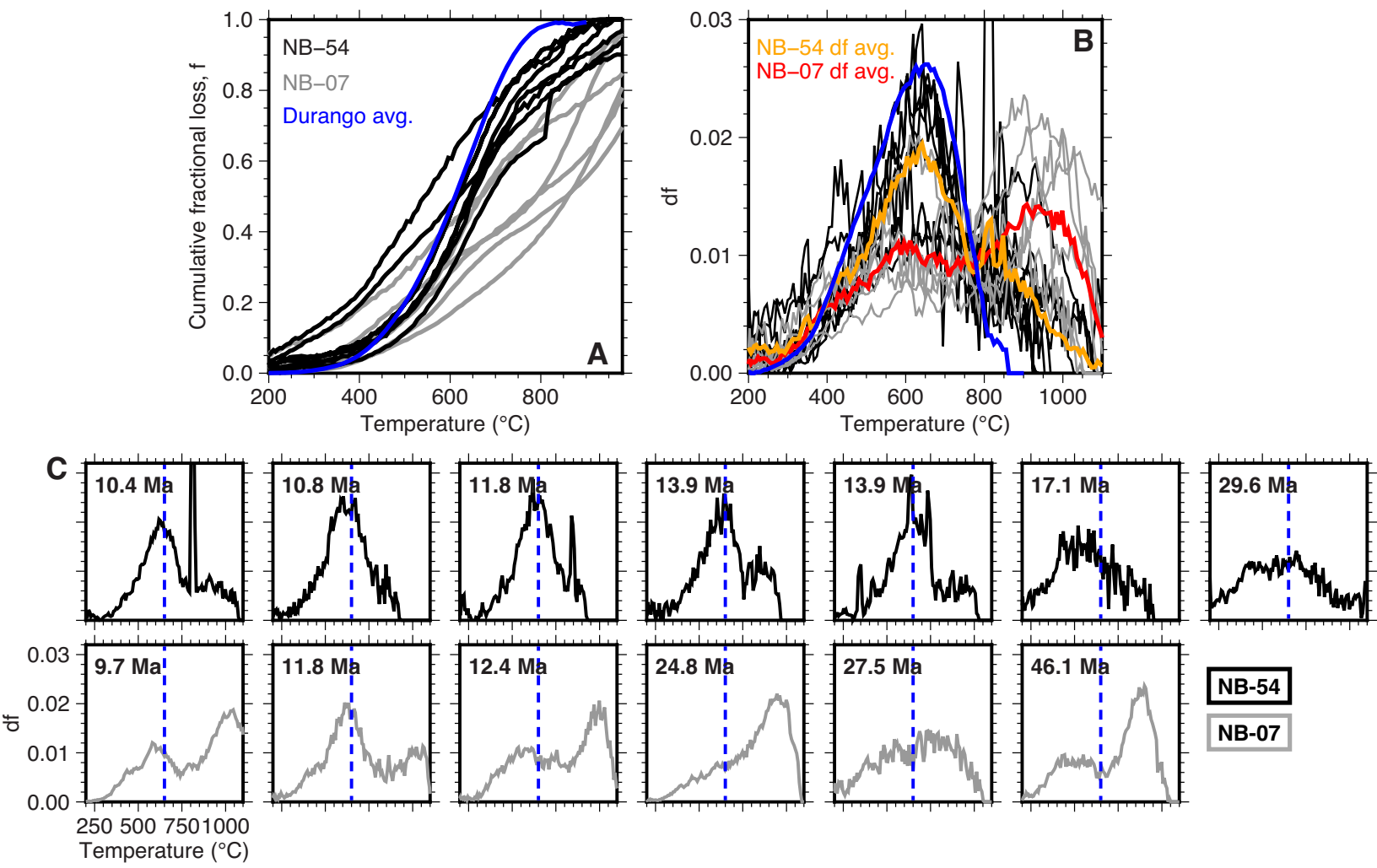
A
Cumulative fractional loss, f
NB–54
NB–07
Durango avg.
Temperature (°C)
B
df
NB–54 df avg.
NB–07 df avg.
Temperature (°C)
C
10.4 Ma
10.8 Ma
11.8 Ma
13.9 Ma
13.9 Ma
17.1 Ma
29.6 Ma
9.7 Ma
11.8 Ma
12.4 Ma
24.8 Ma
27.5 Ma
46.1 Ma
NB-54
NB-07
df
Temperature (°C)

Figure6

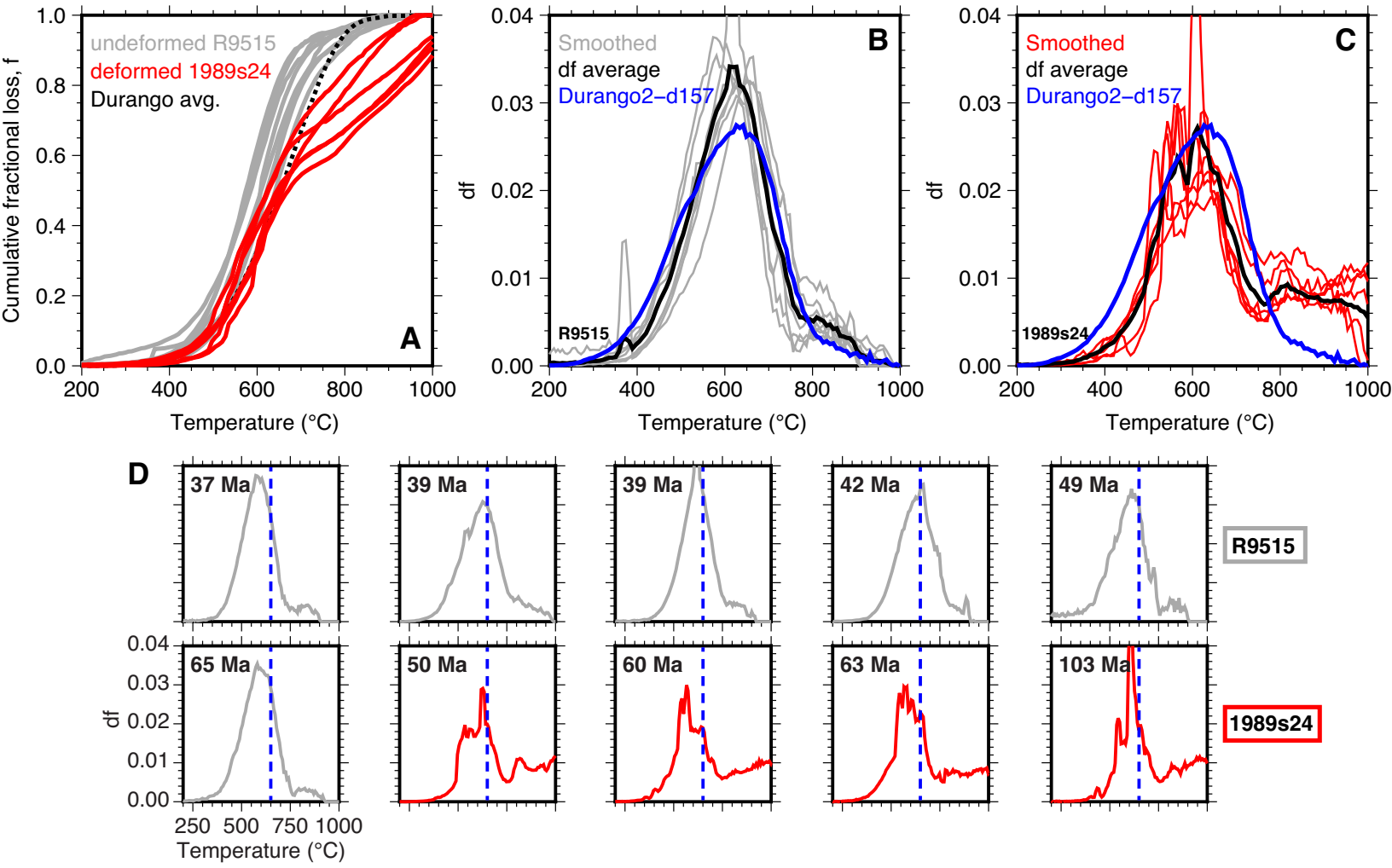
undeformed R9515
deformed 1989s24
Durango avg.
A
Cumulative fractional loss, f
Temperature (°C)
Smoothed
df average
Durango2–d157
B
R9515
df
Temperature (°C)
Smoothed
df average
Durango2–d157
C
1989s24
df
Temperature (°C)
D
37 Ma
39 Ma
39 Ma
42 Ma
49 Ma
65 Ma
50 Ma
60 Ma
63 Ma
103 Ma
R9515
1989s24
df
Temperature (°C)

Figure7

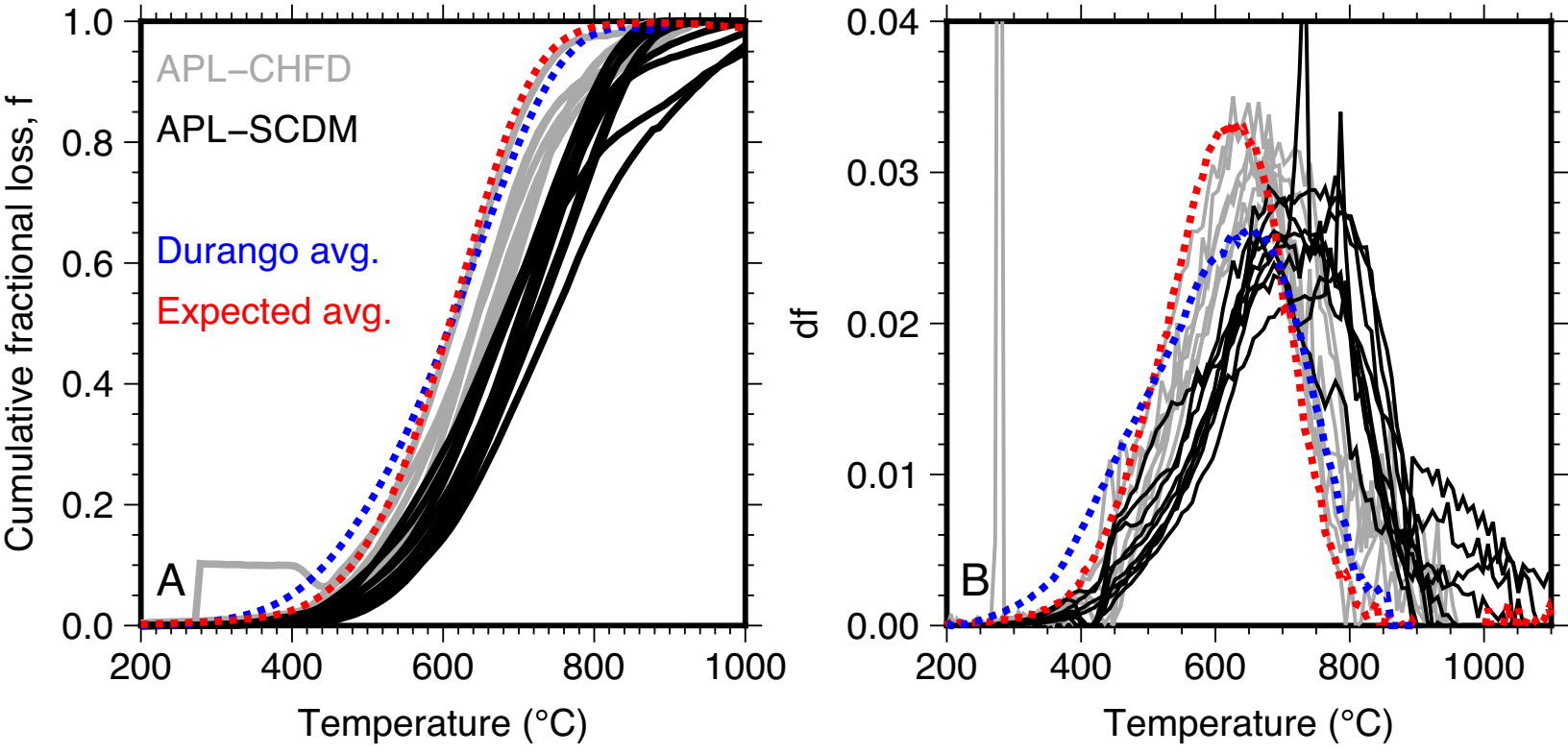
APL–CHFD
APL–SCDM
Durango avg.
Expected avg.
A
B
Cumulative fractional loss, f
df
Temperature (°C)
Temperature (°C)
1.0
0.8
0.6
0.4
0.2
0.0
0.04
0.03
0.02
0.01
0.00
200
400
600
800
1000

Figure8

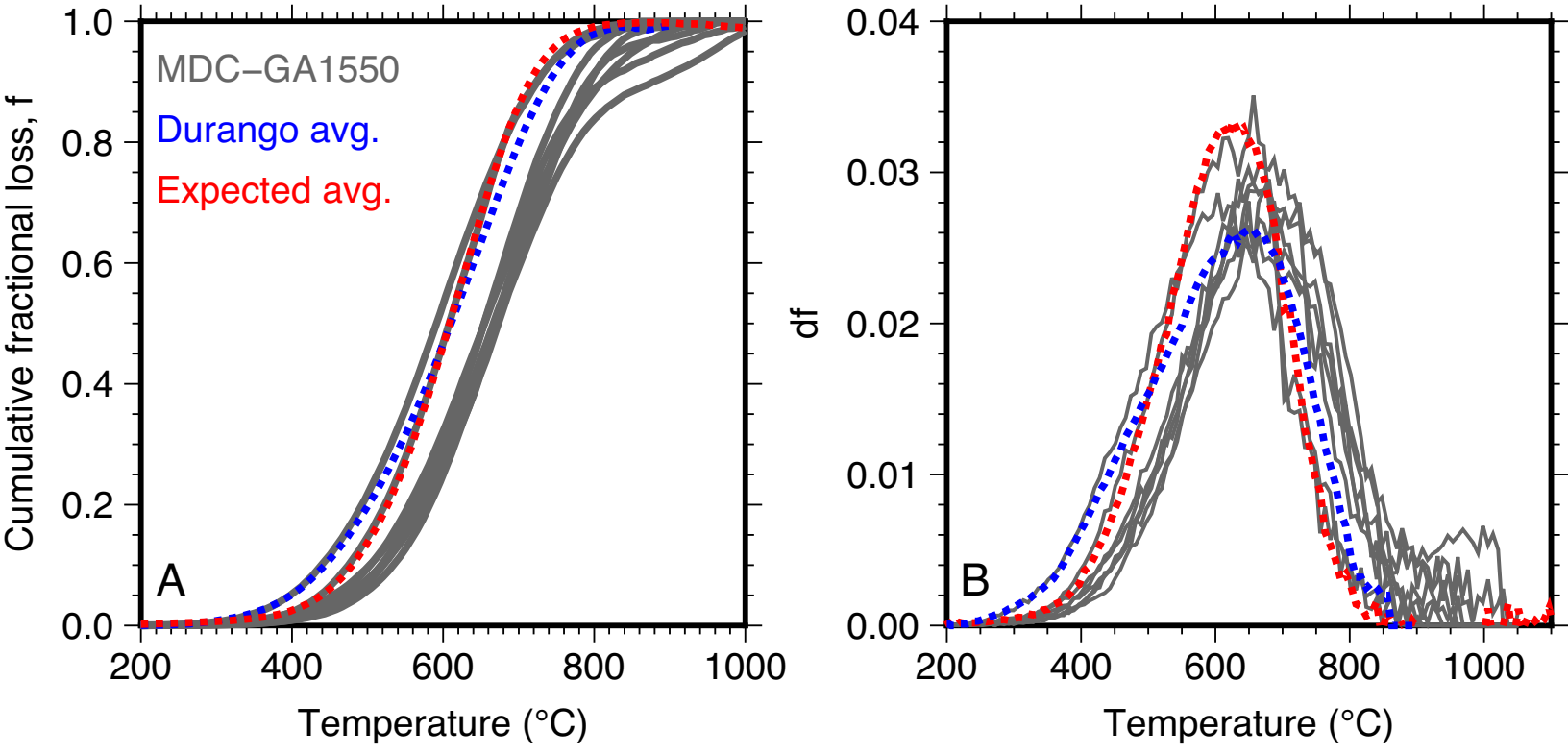
MDC–GA1550
Durango avg.
Expected avg.
A
B
Cumulative fractional loss, f
df
Temperature (°C)
Temperature (°C)
1.0
0.8
0.6
0.4
0.2
0.0
0.04
0.03
0.02
0.01
0.00
200
400
600
800
1000

Figure9

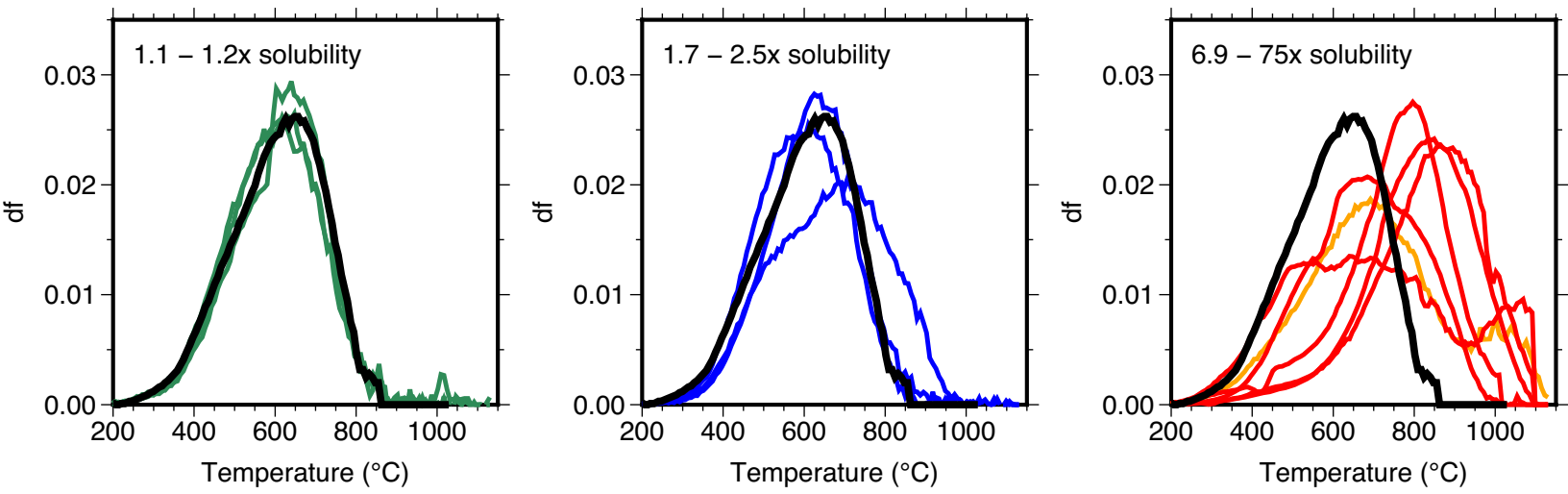
1.1 – 1.2x solubility
1.7 – 2.5x solubility
6.9 – 75x solubility
df
0.00
0.01
0.02
0.03
200
400
600
800
1000
Temperature (°C)

Figure10

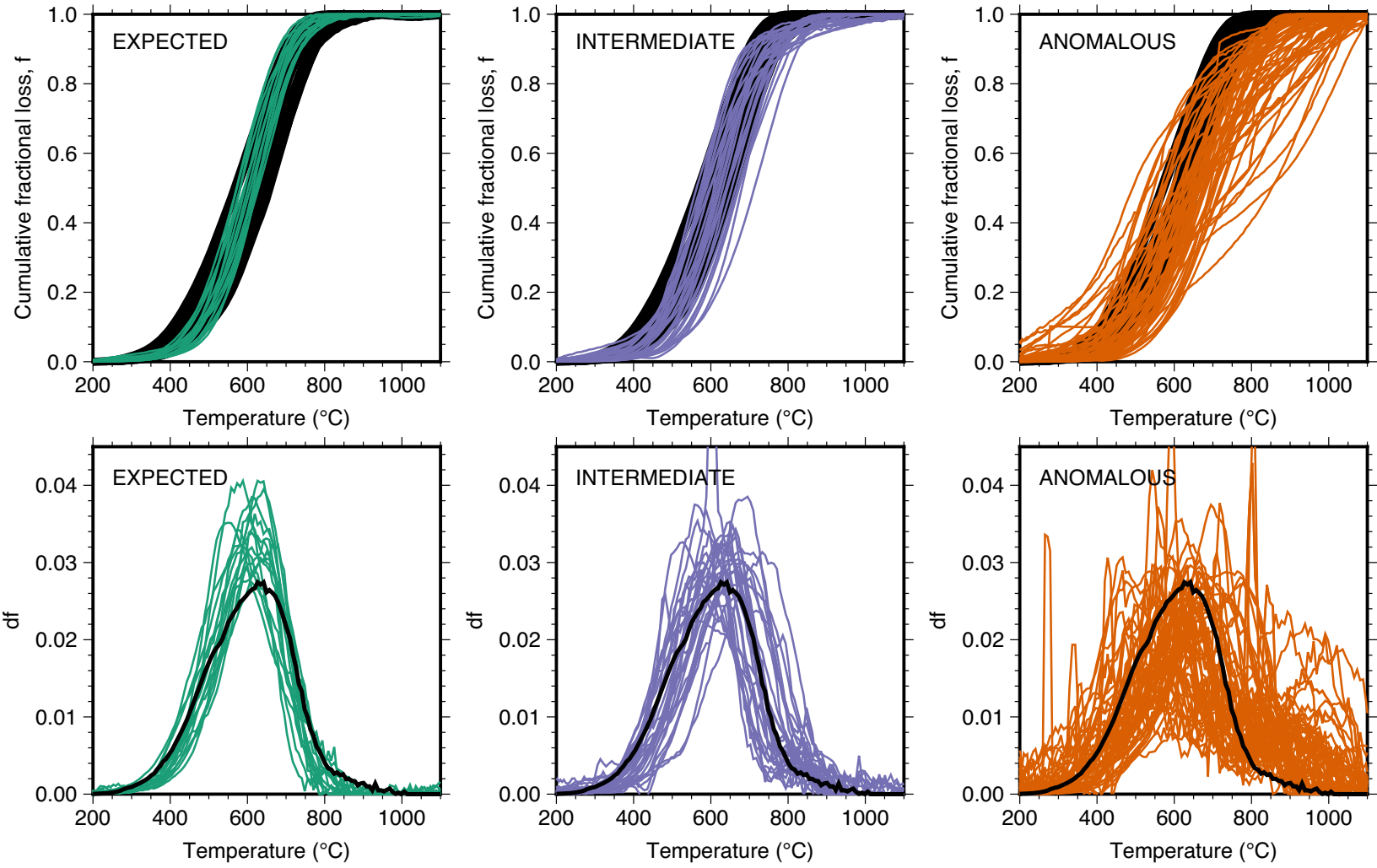
EXPECTED
INTERMEDIATE
ANOMALOUS
Cumulative fractional loss, f
df
Temperature (°C)
0.0
0.2
0.4
0.6
0.8
1.0
0.00
0.01
0.02
0.03
0.04
200
400
600
800
1000

Figure11

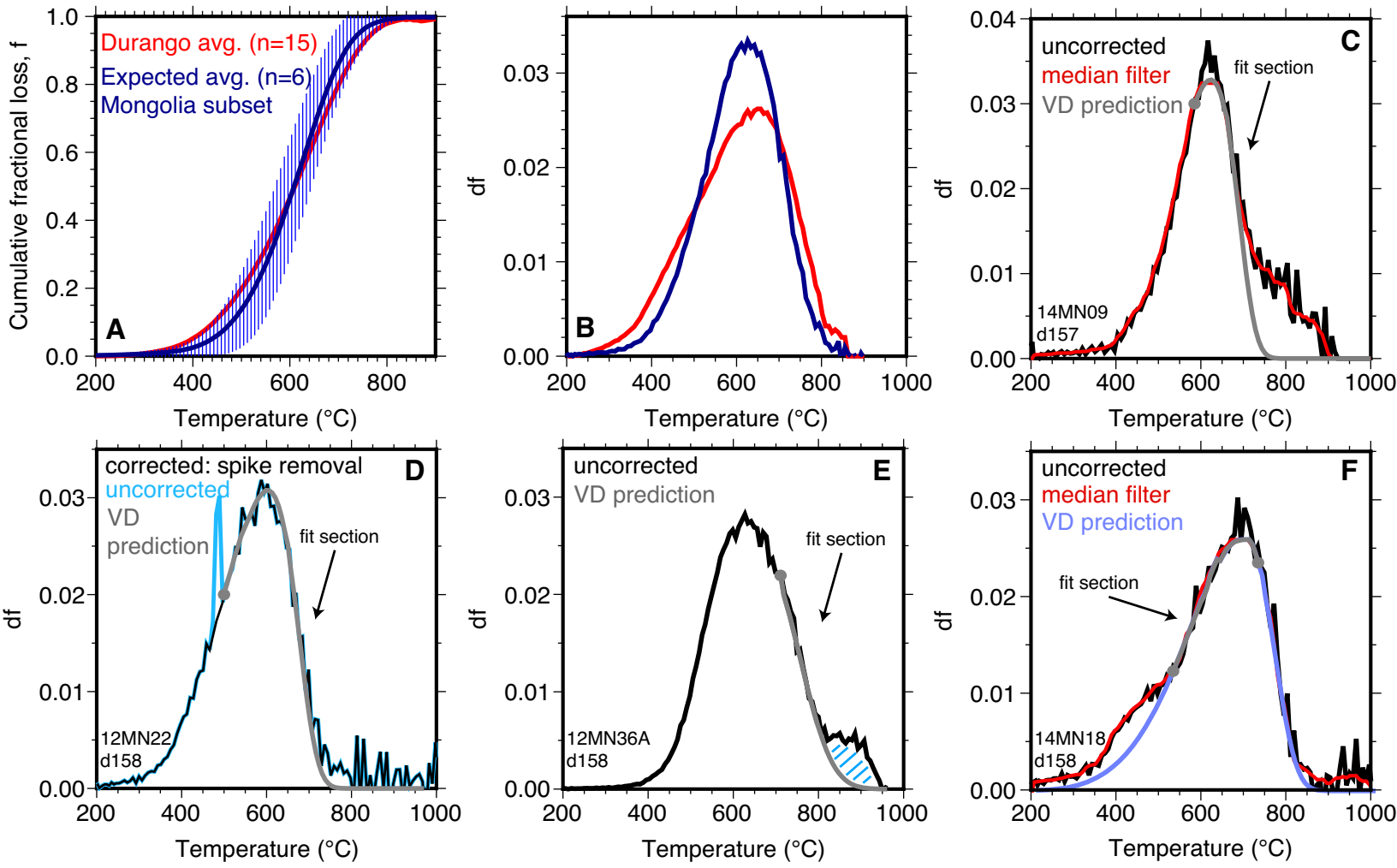
Cumulative fractional loss, f
Durango avg. (n=15)
Expected avg. (n=6)
Mongolia subset
A
Temperature (°C)
df
B
C
uncorrected
median filter
VD prediction
fit section
14MN09
d157
D
corrected: spike removal
uncorrected
VD
prediction
12MN22
d158
E
12MN36A
d158
F
14MN18
d158

Figure12

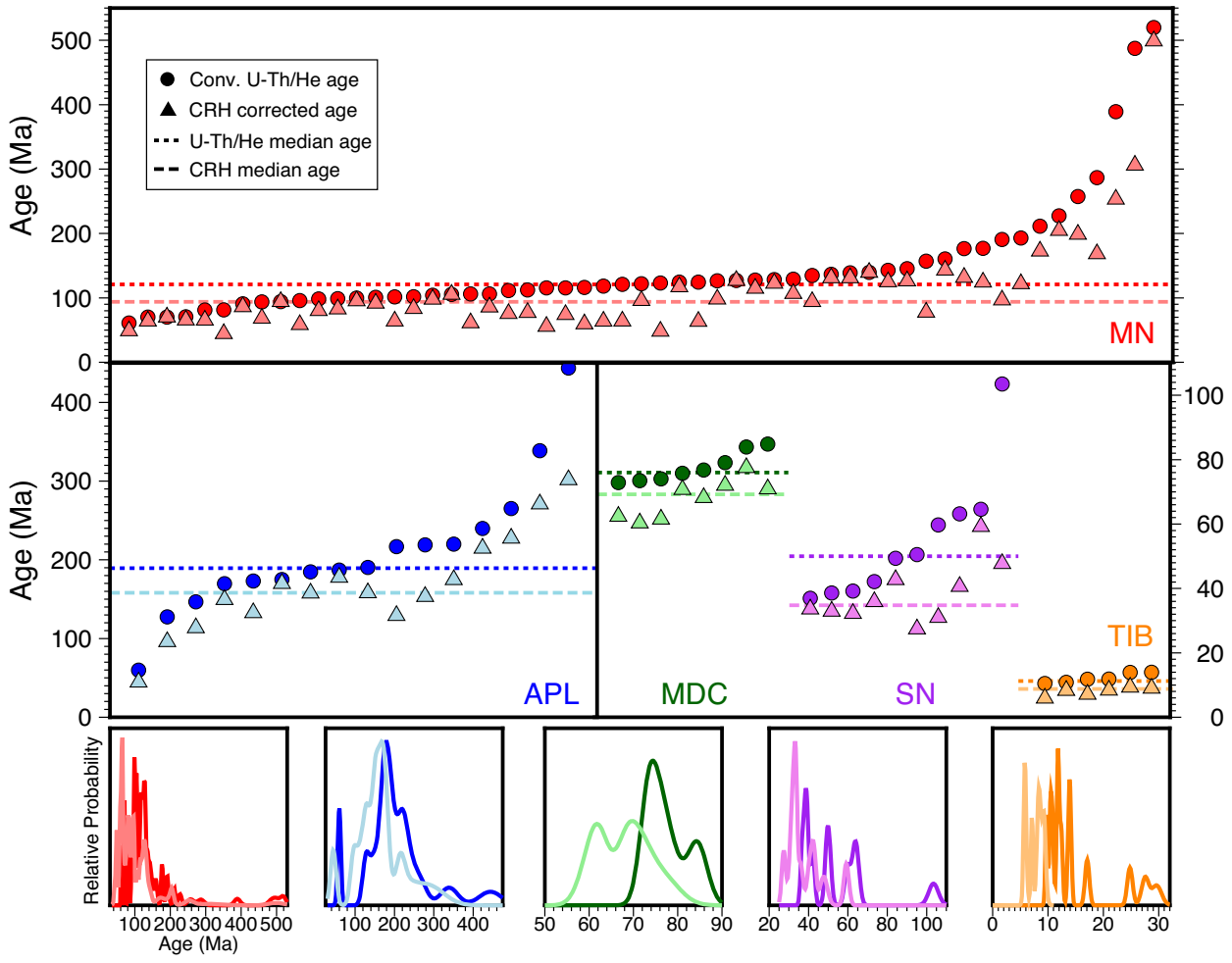
Conv. U-Th/He age
CRH corrected age
U-Th/He median age
CRH median age
Age (Ma)
MN
APL
MDC
SN
TIB
Relative Probability
Age (Ma)